POLITECNICO DI MILANO

Facoltà di Ingegneria dell'Informazione

Corso di Laurea in
Ingegneria delle Telecomunicazioni

Tropospheric scintillation effects: 3D/2D analytical and numerical approaches under spherical wave formalism

Relatore: Prof. Carlo RIVA

Co-relatori: Ing. Vincent FABBRO, Prof. Laurent FERAL

Tesi di Laurea di:

Alessandro TALARICO Matr.783304

Anno Accademico 2012 - 2013

INDEX

LIST OF FIGURES

Sommario

Quando un’onda elettromagnetica attraversa l’atmosfera, ampiezza e fase subiscono rapide variazioni causate dal repentino cambiamento delle disomogeneità del mezzo. Questo fenomeno è definito *Scintillazione* ed è legato alle fluttuazioni di piccola scala dell’indice di rifrazione che sono solite avvenire in ogni regione dell’atmosfera. Sebbene esse non siano singolarmente di grande intensità, possono avere un effetto cumulativo per lunghe distanze. E’ quindi necessario stimare variazioni di ampiezza e fase indipendentemente dalla geometria e dalle caratteristiche elettromagnetiche del collegamento.

Lo scopo del lavoro è di predire tali variazioni statistiche introdotte dalla troposfera, utilizzando un approccio basato su un’onda sferica incidente su uno strato di turbolenza che si trova in una posizione qualsiasi del collegamento. Si analizzeranno in parallelo le configurazioni 2D e 3D e il conseguente errore introdotto dalla riduzione dimensionale. Verranno studiati due metodi: analitico e numerico. Il primo è basato sul calcolo integrale della varianza di ampiezza e fase del segnale valido solo in condizione di debole dispersione, mentre il secondo è basato sul cosiddetto Spit Step Fourier Algorithm (SSF) e si applica in qualsiasi condizione di dispersione.

Parole chiave: spettro delle turbolenze, onda sferica, distribuzione della turbolenza a strato, 3D/2D, Varianze di log-ampiezza e fase, Parabolic Wave Equation (PWE), Split Step Fourier Algorithm (SSF), regimi di Fresnel e Fraunhofer,

Introduction

When an electromagnetic wave passes through the atmosphere, amplitude and phase suffer fast fluctuations caused by inhomogeneity of the medium: this phenomenon is called *Scintillation.* It is related to small-scale turbulent fluctuations of the refractive index that are likely to develop in any region of the atmosphere. Even though these perturbations may be small in magnitude, they can have a significant cumulative effect at long distances. It is therefore necessary to estimate amplitude and phase fluctuations whatever the geometry and the radio-electric characteristics of the link.

For frequencies below 3GHz, ionospheric scintillation is significant while at Ka-band frequencies, scintillation primarily originates in the troposphere. It limits the performances of electromagnetic systems (GNSS systems in L band, earth-satellite telecommunication links, satellite to satellite link in occultation geometry, space-borne Synthetic Aperture Radar…).

So far mainly configurations considering an incident plane wave illuminating a turbulent medium have been taken into account, with first works based on stars' twinkling due to the inhomogeneity of the atmosphere [1] and recently [2][3][4]. Unfortunately this is not a correct approach if the turbulence is near the source because plane wave is only an approximation valid at long ranges.

The object of the work is to predict statistical variations of the electromagnetic signal in troposphere using the more precise approach for an incident spherical wave and any position of the perturbations. We analyse in parallel 3D and 2D modelling and the consequent error due to dimensional reduction. This is done because, although 3D is the real case, 2D is really useful to drop computational cost of numerical simulations. The dimensional reduction is classically used but its effects have been quantified for the plane wave formalism only. The exercise is performed using analytical and numerical methods and convergence of the approaches is studied. The first one is based on integral calculations for the statistical variances of the phenomenon valid for weak scattering only; the second one is based on the split step algorithm (see illustration in Fig.0.1) and it is applied for whatever the scattering condition. Both theories are presented in details with the assumptions taken into account for our situation.

In Chapter 1 we introduce the propagating random medium, i.e. the troposphere, and the statistical part of the refractive index which leads to the formulation of the spectrum of the turbulence.

In Chapter 2 analytical formulations will be derived for log-amplitude and phase variances of a signal propagating through perturbations localized in a thick layer between transmitter and receiver. They are studied with respect to the frequency, the path length and the dimension of the eddies, and with respect to the configuration, 2D or 3D.

In Chapter 3 we present a comparison with the results found so far about the incident plane wave, adding comments of our formulations of the previous chapter.

In Chapter 4 starting from Parabolic Wave Equation (PWE) we develop our model based on the Split Step Fourier algorithm (SSF) and spherical phase screens scheme (3D PWE-2D MPS and 2D PWE-1D MPS).

In Chapter 5 we show our numerical simulations, comparing the analyses of the previous chapters.

Finally we summarize the conclusions of our work, giving some perspectives.

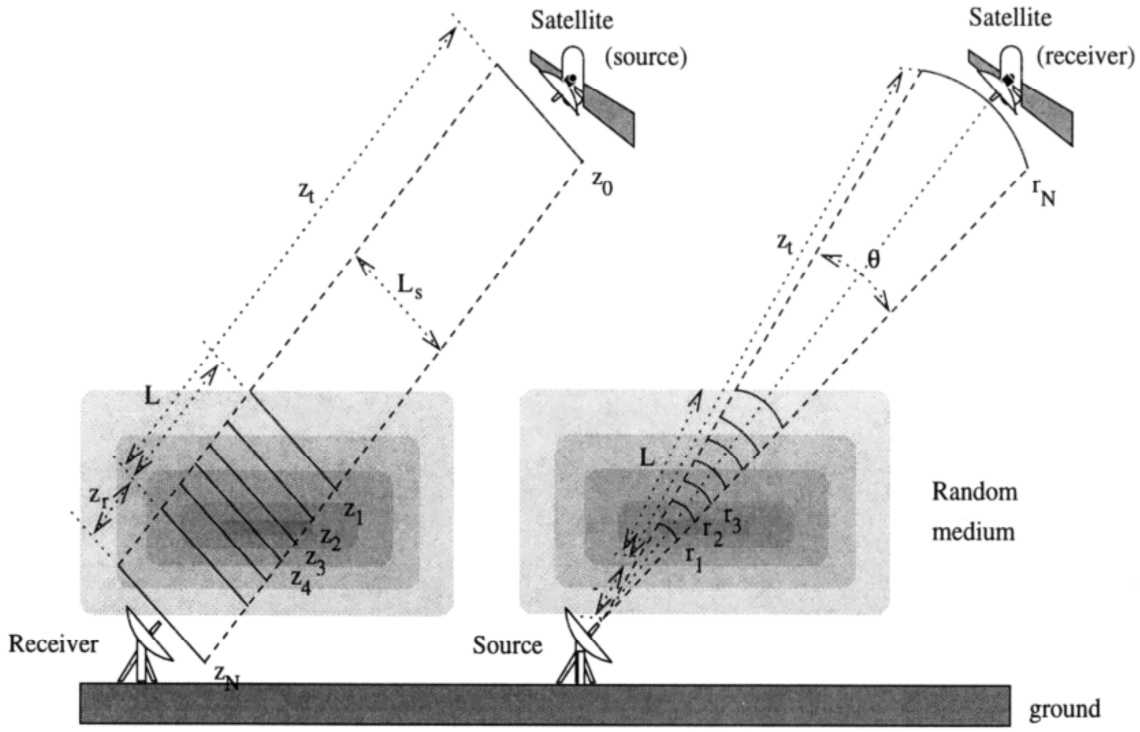

Figure 0.1: Communication system between a Satellite and an Earth station with propagation in a random media (troposphere). On the left side the scheme of the classical studies based on plane wave, on the right our scheme based on spherical wave, which is more correct when the turbulence is close to the emitter [30].

Chapter 1

Description of the propagation medium

Propagation of satellite signals through a large striated region presents the problem of radio-wave propagation through a thick medium composed of random fluctuations in the index of refraction. The wave firstly suffers random phase perturbations due to variations in the phase velocity within the medium. These phase variations in the propagating wavefront introduce small random changes in the direction of propagation of the wave. Thus portions of the initial wavefront now propagate in different directions relative to other portions. As the wave propagates further, diffraction or angular scattering causes constructive and destructive interference which introduces fluctuations in amplitude as well as phase. This is what we define as scintillation. These time-varying amplitude and phase fluctuations represent an undesired complex modulation of the carrier.

In this section we propose an introduction as the base of the work, showing the cause of scintillation in the medium of our interest, i.e. the troposphere.

1.1 Long term variations of the refractive index in the troposphere

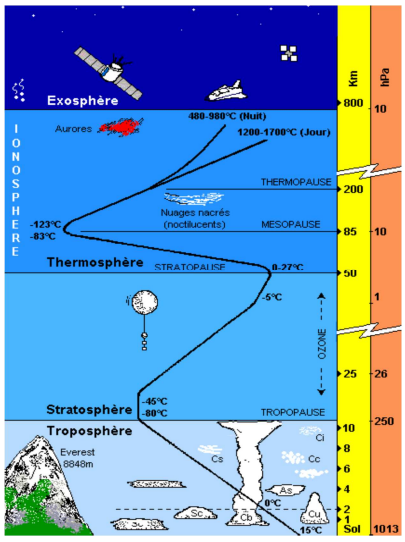

Figure 1.1:Vertical structure of the atmosphere

Troposphere is the region of the atmosphere spreading from the ground up to an altitude of 7 to 14km (Fig.1.1), depending on the latitude and the meteorological conditions. This is the place where the atmospheric phenomena involve the water cycle (cloud, rain, fog, snow).

From an electromagnetic point of view, the troposphere is a pure dielectric medium (electric conductivity σ=0, magnetic permeability μ=μ_o and imaginary part of the dielectric constant ε'' negligible with respect to the real part ε') except for the shortest wavelengths, i.e. centimetric and millimetric, for which it can be more or less absorbing.

In the troposphere, temperature, humidity and pressure vary horizontally and vertically, generating variations of the air refractive index. The average vertical variations of the tropospheric refractive index are described by the large scale effect:

$$n(h) = n_o(1 + B \times h) \tag{1.1}$$

where n is refractive index at an altitude h(km), n_o is the refractive index at sea level and B is given by Booker's formula:

$$B = \frac{1}{R_o}\left(-0.2 + 30\frac{dP}{dh} - 6\frac{dT}{dh}\right) \qquad [m^{-1}] \tag{1.2}$$

where R_o=6400 km is the Earth radius, $\frac{dP}{dh}$ ($\frac{dT}{dh}$) is the variation of atmospheric pressure (temperature) with height (mbars/m and °C/m, respectively).

As n_o is very close to 1 ($n_o \approx 1$) et Bh<<1, the equation (1.1) becomes:

$$n(h) = n_o + B \times h \tag{1.3}$$

and the tropospheric refractive index n(h) remains very close to unity (it is about 1.0003 close to the surface of the Earth). Nevertheless, its vertical gradient impacts the electromagnetic wave propagation. Therefore, it has become customary to use the refractivity N:

$$N = (n-1).10^6 \tag{1.4}$$

which can be approximated by:

$$N = \frac{77.6}{T}\left(p + 4810\frac{e}{T}\right) \tag{1.5}$$

where p is the atmospheric pressure (hPa), e is the partial pressure of water vapour (hPa), T the temperature (K).

At the tropopause (about 15km in temperate latitudes), N is about 40, down from over 300 at the surface. The relative differences resulting from humidity variations are much stronger near the surface. This explains why scintillation generally originates in the lower levels of the troposphere. Even when turbulence does occur in the upper levels of the atmosphere, the relative differences in refractive index between adjacent air masses are insignificant compared with that seen near the surface in the atmospheric boundary layer.

The atmosphere is generally stratified into parallel layers by temperature and humidity differences. Turbulence within a layer will generate very little scintillation because the air is fairly well mixed within the layer and refractive differences are small. However, at the boundaries between layers, turbulence can mix air masses with very different characteristics. This phenomenon allows scintillation to be modelled to a first approximation as occurring in a thin layer or layers, with the rest of the propagation path assumed to be scintillation free [5].

Tropospheric scintillation can occur under several distinct circumstances. Turbulence in the lower troposphere can cause random mixing between air masses, resulting in dry scintillation (also referred to as clear air scintillation). Note that “dry” in this context does not mean that water vapour is not present; there is always a finite amount of water vapour in the troposphere. Rather, “dry” merely means that the air is not saturated by water vapour. When water vapour saturation does occur, clouds are formed. As the clouds pass through the propagation path, scintillation can occur at the boundary between the cloud and the clear atmosphere. Since this involves air which is saturated by water vapour, this is called wet (or moist) air scintillation [6]. Given the right conditions, cloud droplets condense to produce rain within the propagation path. Variations in rainfall within the propagation path cause signal variations which constitute another source of scintillation [7].

Regardless of the cause, scintillation-induced signal variations generally have a period of a few seconds. This distinguishes scintillation from slow-fading rain attenuation events which have periods of several minutes [8]. Also, in contrast to rain fading, it should be noted that scintillation is not a loss process. The scintillation variations cause both enhancement and attenuation of the propagating signal, but the average signal level remains unchanged. Scintillation may occur simultaneously with rain attenuation, but the two effects are caused by different mechanisms [9]. Clear-air scintillation is the result of turbulent mixing in the troposphere, while rain attenuation is caused by the absorption and scattering of electromagnetic energy by liquid raindrops.

Therefore, spatial-temporal variations of the refractive index are complex and cannot be known from a deterministic point of view, so we introduce a statistical description of the medium.

1.2 Spectral description of the small scale fluctuations of the refractive index

The refractive index $n(\vec{r},t)$ is commonly described by a stochastic function of the position $\vec{r} \equiv (x, y, z)$ and time t. $n(\vec{r},t)$ is classically decomposed as:

$$n(\vec{r},t) = < n_0 > + n_1(\vec{r},t) \tag{1.6}$$

where $< n_0 >$ is the average component responsible for the large scale refraction effects and $n_1(\vec{r},t)$ the random turbulent component.

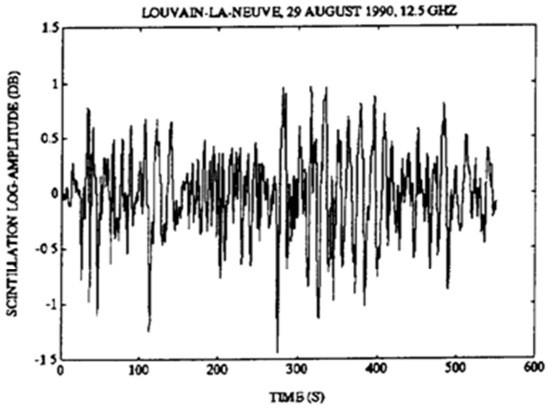

Figure 1.2: Amplitude scintillations of a satellite signal at12.5 GHz received at Louvain (Belgium)[10]

The fast fluctuation, at small scale, of $n_1(\vec{r},t)$ lead to fast fluctuation of the signal around its average value: this is tropospheric scintillation phenomenon illustrated in Fig.1.2.

It is a source of perturbations for the electromagnetic systems: it is thus necessary to have a statistical description of electromagnetic scintillation (Amplitude and phase variances of the signal) to allow an optimal system design.

Disregarding the large scale refraction effects, $< n_0 >$=1 so that (1.6) reduces to:

$$n(\vec{r},t) = 1 + n_1(\vec{r},t) \tag{1.7}$$

Besides, in compliance with various experimental measurements, $n_1(\vec{r},t)$ is a centred random variable $< n_1(\vec{r},t) >$=0 where < > denotes ensemble average.

Lastly, under assumptions of stationary (in time) and homogeneous (in space) turbulent random medium, the 3D spatial covariance function of the turbulent index $< n_1(\vec{r},t) n_1(\vec{r'},t) >= B_{n_1}^{3D}(\vec{r},\vec{r'},t)$

reduces to $B_{n_1}^{3D}(\vec{r}-\vec{r}')$. It is related by 3D Fourier transform to 3D spatial spectrum $S_{n_1}^{3D}(\vec{k}\equiv k_x,k_y,k_z)$ according to:

$$\left\langle n_1(\vec{r},t),n_1(\vec{r}',t)\right\rangle = B_{n_1}^{3D}(\vec{r}-\vec{r}') = \int_{-\infty}^{+\infty} S_{n_1}^{3D}(\vec{k})e^{i\vec{k}(\vec{r}-\vec{r}')}d\vec{k} \qquad (1.8)$$

where $\vec{k}\equiv(k_x,k_y,k_z)=\left(\frac{2\pi}{l_x},\frac{2\pi}{l_y},\frac{2\pi}{l_z}\right)$ is the wavenumber associated to the eddy of dimension l_x x l_y x l_z. Besides, note that the 3D Fourier convention used in (1.8) implies that:

$$S_{n_1}^{3D}(\vec{k}) = (2\pi)^{-3}\int_{-\infty}^{+\infty} d^3r.\, B_{n_1}^{3D}(\vec{r})e^{-i\vec{k}.\vec{r}} \qquad [m^3] \qquad (1.9)$$

For fully developed turbulence, $S_{n_1}^{3D}(\vec{k})$ is classically represented by the Kolmogorov spectrum that relies on a description of the turbulence through an inertial cascade illustrated in Fig.1.3.

As the turbulence spectrum (or simply spectrum, as we will call it hereinafter) is assumed isotropic, instead of $\vec{k}$ it is possible to consider its absolute value $|\vec{k}|=\kappa$.

According to Kolmogorov theory, the spectrum is divided in three zones by two important parameters: the wavenumbers $K_{is}=2\pi/l_{is}$ [rad/m] and $K_{os}=2\pi/L_{os}$ [rad/m], where l_{is}[m] and L_{os}[m] are inner and outer scales of turbulence respectively.

These two extreme lengths are important for the angle of diffraction which strictly depends on the size of the scatterer: smaller it is, wider the angle. In addition, the inner scale controls the spatial correlation for small inter-receiver separations and can alter it mostly if comparable to the Fresnel distance $\sqrt{\lambda R}$, where R is the distance transmitter –receiver and λ the wavelength.

A good rule of thumb [11] is that one can ignore dissipation effects when:

$$\sqrt{\lambda R} > 7l_{is} \qquad [m] \qquad (1.10)$$

Since the inner scale is usually less than 1 cm in the troposphere, this distortion should occur only for optical links over distances less than 50 m. It should be completely absent for microwave links, which have much larger Fresnel lengths.

By contrast, L_{os} is equivalent to the correlation distance of refractive index fluctuation and it is used for the definition of two situations which will be taken into account in this work:

Fresnel regime if $\sqrt{\lambda R} << Los$ [m] (1.11)

Fraunhofer regime if $\sqrt{\lambda R} >> Los$ [m] (1.12)

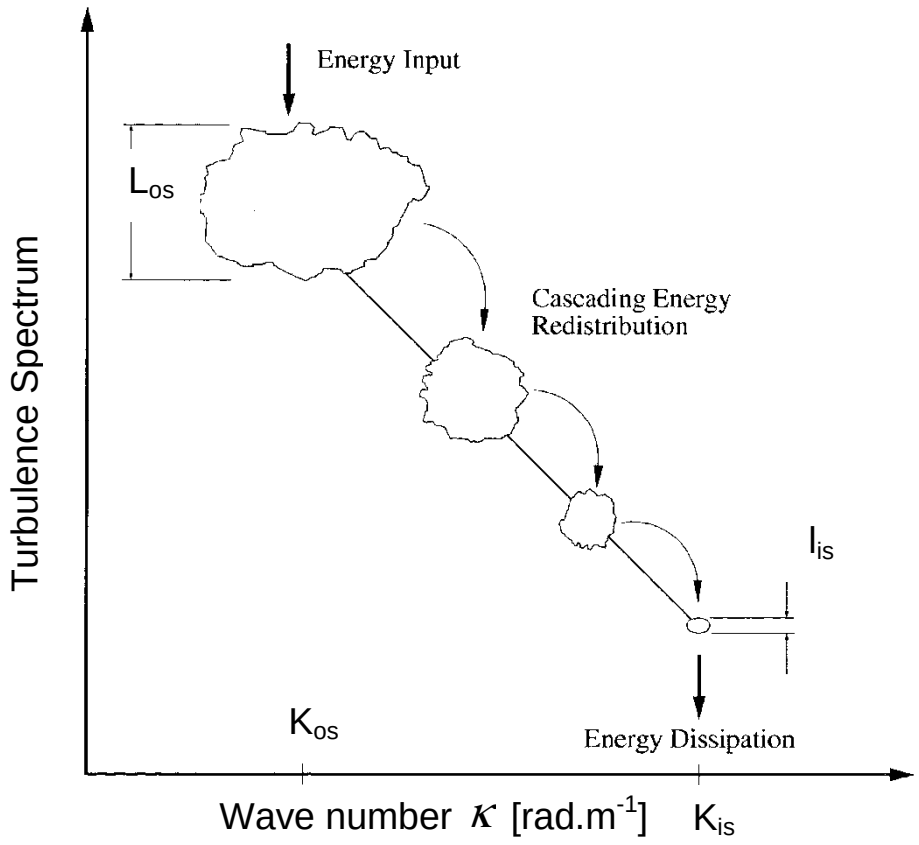

Figure 1.3:Conceptual description of the process of turbulent decay as it proceeds through an energy cascade in which eddies subdivide into progressively smaller eddies until they finally disappear [10].

In other words, comparing our situation to the physical optics, we are considering a scatterer with aperture equal to Los and the ratio $\frac{\sqrt{\lambda R}}{L_{os}}$ the *Fresnel number*. Conceptually, its inverse is the number of half-period zones in the wavefront amplitude, counted from the centre to the edge of the aperture, as seen from the observation point, so that the wavefront phase change by π moving from a half-period zone to another. Fraunhofer regime is established when the diffraction pattern is viewed at a long distance from the diffracting object, in the so called *far field* zone. On the other hand, the diffraction pattern created near the object, in the *near field* region, is dealt with by Fresnel regime.

The three regions of the spectrum are shown in Fig.1.4. The abscissa is the value $\frac{2\pi}{l}$[rad/m], where l is the eddy size. They are defined as:

- *Input range* ($l \geq L_{os}$)

  The energy is introduced into the turbulence in this range of eddy sizes due to the wind shear and temperature gradient. The spectrum depends on how the turbulence is created for the particular case, and thus there is no general formula describing the turbulence characteristics in this range

- *Inertial sub-range* ($L_{os}>l>l_{is}$)

  The kinetic energy of eddies dominates over the dissipation due to viscosity, and the turbulence is essentially isotropic. The spectrum is proportional to $|\vec{k}|^{-11/3}$. Kolmogorov theory.

- *Dissipation range* ($l \leq l_{is}$)

  Here the dissipation of energy due to viscosity dominates over the kinetic energy, and therefore, the spectrum is extremely small

For the reasons just exposed, in the first region the spectrum is unknown. In the second one we have:

$$\boxed{S_{n_1}^{3D}\left(\left|\vec{k}\right|\right) = S_{n_1}^{3D}(\kappa) = 0.033 C_n^2 \kappa^{-11/3}} \qquad [m^3], \qquad (1.13)$$

which is Kolmogorov spectrum.

C_n^2 is the turbulent constant structure that accounts for the turbulence strength, and it ranges typically between 10^{-18} $m^{-2/3}$ (weak turbulence) and 10^{-12} $m^{-2/3}$ (strong turbulence). It has been mathematically derived by Ishimaru ([12] app. C) and can be expressed in function of the variance of n_1 [11]:

$$C_n^2 = 1.91 \left\langle n_1^2 \right\rangle K_{os}^{\frac{2}{3}} \qquad [m^{-\frac{2}{3}}] \qquad (1.14)$$

Where variance $\sigma_n^2 = \left\langle n_1^2 \right\rangle$ because $\langle n_1 \rangle = 0$.

Finally in the third region:

$$S_{n_1}^{3D}(\kappa) \approx 0 \qquad [m^3] \qquad (1.15)$$

L_{os} and l_{is} are respectively a few millimetres and some hundreds of meter in the atmosphere.

Von Karman [13] proposed an analytical extension of the Kolmogorov spectrum:

$$\boxed{S_{n_1}^{3D}(\kappa) = 0.033 C_n^2 \left(\kappa^2 + K_{os}^2\right)^{-11/6}} \qquad [m^3] \qquad (1.16)$$

Which assigns a reasonable spectral shape for every wave-number, even in the energy input regime and it matches to Kolmogorov model in the inertial subrange.

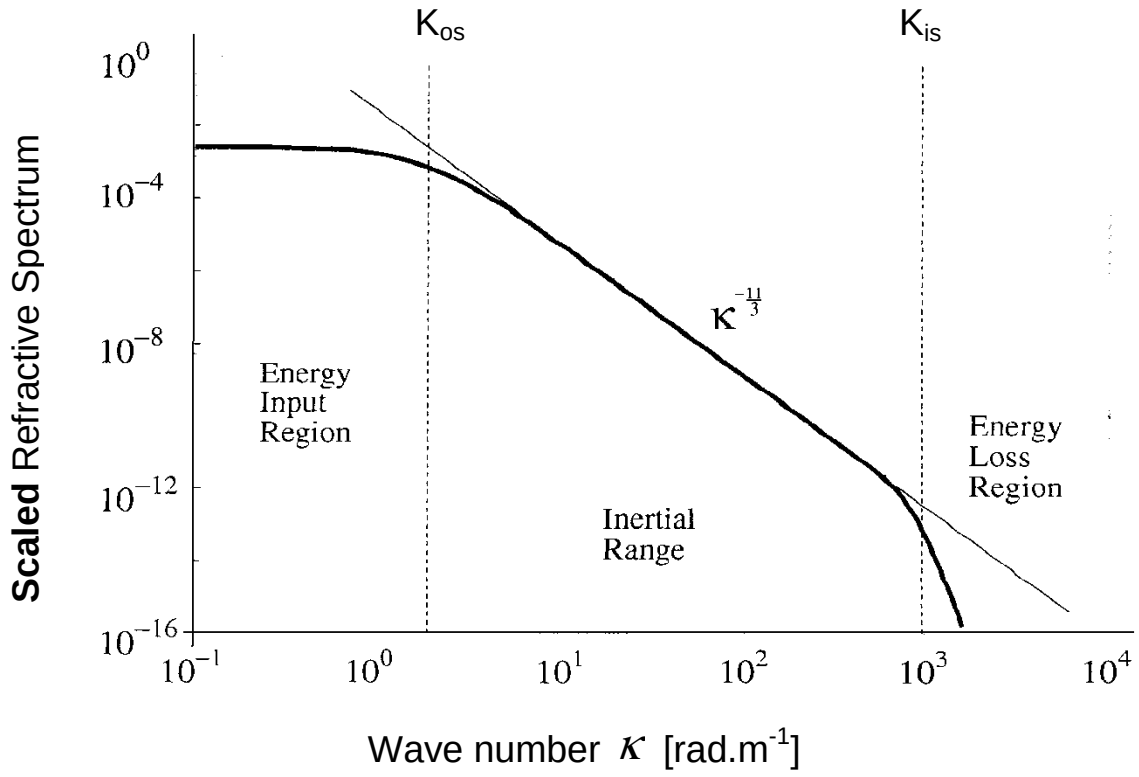

Figure 1.4: Normalized representation $S_{n_1}^{3D}(|\vec{k}|)/C_n^2$ *of the Von Karman spectrum[10]*

Chapter 2

Analytical derivations

After a brief introduction of the propagating medium, analytical expressions for amplitude and phase variances are computed. The scenario concerns a turbulence limited in a part of the link, where scintillations effects take place. This is the so called 'Layer distribution model' in contrast with 'slab model' where the turbulence spreads from the transmitter to the receiver.

Practical situation involved the uplink of a satellite communication or a classical terrestrial link, when the irregularities are near the point source and the incident wave is spherical.

We start the discussion introducing random wave equation under weak scattering condition with an approximation discovered by Rytov, who was analysing the diffraction of light by sound waves [14], later applied by Obukhov to describe the propagation of electromagnetic waves in random media [15]. This technique is now known alternatively as the method of smooth perturbations or the Rytov approximation, which is widely used to describe line-of-sight propagation in turbulent media when the amplitude variations are small [11][16]. The Rytov approximation is fundamentally an enlargement of geometrical optics that includes diffraction effects. The essence of this method is to express the field strength as the product of the unperturbed field and the exponential of a surrogate function, which must be determined. It is a complex function that describes the important influence of diffraction because it is derived from the random-wave equation. To solve specific transmission problems one expands the surrogate function in powers of dielectric variation $\delta\varepsilon$. Most descriptions of propagation rely on this basic solution. Pisereva showed that the variance of logarithmic amplitude variations must be less than unity in all situations [17].

Rytov condition: $\langle \chi^2 \rangle < 1$ [Np²] (2.1)

Tatarskii confirmed it with explicit calculations [1] and Pisareva showed that the phase is unbounded for the usual case of Fresnel scattering [17]. This condition gives us the flexibility required to characterize weak scattering, which is equivalent to the assumption that the beam can be scattered by the eddy only once. In the hierarchy of propagation theories researchers are developing, the Rytov approximation represents a natural stopping point between geometrical optics and modern theories of strong fluctuations: it describes some features of multiple scattering, just as geometrical optics does, on the other hand it can describe weak fluctuations in amplitude and intensity – which geometrical optics cannot. We shall show that its results reduce to those of geometrical optics when the influential

scatterers are concentrated near the ray-path of the unperturbed field. It captures the influence of diffraction phenomena. Phase fluctuations appear naturally in the exponent of the Rytov solutions and can be very large for most applications.

Under weak scattering condition, we solve random wave equation getting a function which is fundamental for our study because it allows describing how the field is scattered and because it has to filter the spectrum of turbulences: we will define it as “weighting function”. With the latter and the spectrum defined in the Chapter 1, it will be possible to compute the variances.

2.1 Variances for the real 3D configurations

2.1.1 Variances definition under weak scattering assumption

Maxwell equations in a random medium are hard to solve because of the complexity of the system deriving from variability of the coefficients involved in the equations.

They concern:

1) Time domain

- Wave is monochromatic

- Propagation is in harmonic regime and temporal variations inside the medium are much slower than a wave period. It implies that a wave sees constant irregularities

- l is the dimension of the inhomogeneity to the direction of propagation. First theoretical studies [18] have been done for plane wave in optical domain where $l >> \lambda$. The medium is supposed to vary slowly so that the refractive index is assumed constant on the signal wavelength. This assumption allows to suppress the time dependency on Electromagnetic Field in Maxwell’s equation.

- given short time for the wave to cross the medium, perturbation is considered stationary.

2) Spatial domain

- We use paraxial approximation assuming a wave propagating along the axis so that all the energy is diffused forward in a narrow cone [18], neglecting backscattering and power absorption by the medium. In Fig.2.1 we show an incident wave diffracted in a limited angle $\vartheta = \frac{\lambda}{l}$[rad], where l is the transverse dimension of a generic scatterer which is at distance L from the receiver. Until the diffraction spot $L\vartheta$ is less than l, diffractive effects are negligible

and only phase is affected. Thus the influence of the medium depends on the average dimension of inhomogeneity in relation with the wavelength. This hypothesis is the basis of a lot of other approximations like the one driven by Markov which allows parabolic method starting from classical wave equation.

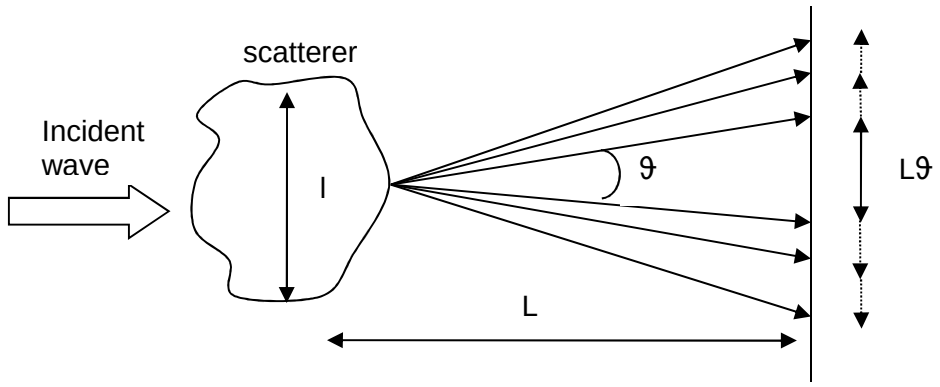

Figure 2. 1:Geometry of diffraction. Until the spot Lϑ < l diffractive effects are negligible

3) Phenomena neglected

- Depolarization effects.

It has been found experimentally that inhomogeneities of troposphere induce scintillation independently from polarization. This point allows us to use a scalar wave equation instead of vector one.

- Ground effect.

Reflection or diffraction phenomena, caused by the terrain, affect the downlink communication, but here we want to focus on the effect generated by the tropospheric layer so we neglect them.

- Multi-path.

Diffusion and diffraction due to obstacles are not considered.

Under these basic assumptions it is possible to derive the calculations.

In harmonic regime, Maxwell equations referred to Electric and Magnetic fields are:

$$\nabla x\vec{E}(\vec{r}) = i\omega\mu_0\vec{H}(\vec{r}) \tag{2.2}$$

$$\nabla x\vec{H}(\vec{r}) = -i\omega\varepsilon_0\varepsilon_r\vec{E}(\vec{r}) \tag{2.3}$$

Where E and H are respectively electric and magnetic fields, $w = 2\pi f$, $\varepsilon_0 = 8.854187817 \times 10^{-12} \mathrm{Fm}^{-1}$

and $\mu_0 = 4\pi \times 10\text{-}7\ \mathrm{Hm}^{-1}$ dielectric and permeability constant of the vacuum and finally ε_r the dielectric constant of the medium depending on the position. Troposphere is assumed with no free charges so implicitly $\mu_r = 1$.

Solving the system of the two previous equations we get:

$$\nabla x \nabla x \vec{E}(\vec{r}) - \omega^2 \mu_0 \varepsilon_0 \varepsilon_r \vec{E}(\vec{r}) = 0 \tag{2.4}$$

Noting that:

$$\nabla x \nabla x \vec{E}(\vec{r}) = -\nabla^2 \vec{E}(\vec{r}) + \nabla\left(\nabla \cdot \vec{E}(\vec{r})\right) \tag{2.5}$$

And

$$\nabla \cdot \left[\varepsilon_r(\vec{r})\vec{E}(\vec{r})\right] = 0 \tag{2.6}$$

equation (2.4) becomes:

$$\nabla^2 \vec{E}(\vec{r}) + \omega^2 \mu_0 \varepsilon_0 \varepsilon_r(\vec{r})\vec{E}(\vec{r}) - \nabla\left(\frac{\nabla \varepsilon_r}{\varepsilon_r} \cdot \vec{E}(\vec{r})\right) = 0 \tag{2.7}$$

In term of n:

$$\nabla^2 \vec{E}(\vec{r}) + k_0^2 n^2(\vec{r})\vec{E}(\vec{r}) = 2\nabla\left(\frac{\nabla n}{n} \cdot \vec{E}\right) \tag{2.8}$$

On the right side of the equation (2.8) polarization effect appears but, as exposed above, in clear sky conditions, the depolarization effects are negligible. It leads to the scalar wave equation :

$$\nabla^2 E(r) + k_0 n^2(r) E(r) = 0 \tag{2.9}$$

where $k_0 = \frac{2\pi}{\lambda_0}$ is the wave-number in the vacuum with λ_0 wave-length, $E(\vec{r})$ one of the component of the electric-field vector.

Considering the first order approximation for the refractive index n defined in (1.7):

$$n^2 = (1+n_1)^2 \approx 1+2n_1 \tag{2.10}$$

the vector wave equation (2.9) reduces to:

$$\nabla^2 E(r) + k_o^2[1 + 2n_1(r,t)]E(r) = \vec{0} \tag{2.11}$$

We solve this equation under Rytov approximation [14]. It consists in expressing the unknown solution as the product of the field strength $E_o(\vec{R})$ that would be measured at $\vec{R}$ in the absence of turbulent irregularities with a correction term $\psi(\vec{R},t)$ so that:

$$E(\vec{R}) = E(\vec{R},t) = E_o(\vec{R})e^{\psi(\vec{R},t)} \quad . \qquad \text{[V/m]} \tag{2.12}$$

The complex function $\psi(\vec{R},t)$ is then expanded into a series:

$$\psi(\vec{R},t) = \sum_{i=1}^{+\infty} \psi_i(\vec{R},t). \tag{2.13}$$

Under weak scattering assumption, the first term of the series is sufficient to accurately describe the propagation, so that:

$$E(\vec{R},t) \approx E_o(\vec{R})e^{\psi_1(\vec{R},t)}, \qquad \text{[V/m]} \tag{2.14}$$

with:

$$\psi_1(\vec{R},t) = -2k_o^2 \int d^3r G^{3D}(\vec{R},\vec{r}) n_1(\vec{r},t) \frac{E_o(\vec{r})}{E_o(\vec{R})}. \tag{2.15}$$

where it appears the Green function in free space defined as:

$$G^{3D}(\vec{R},\vec{r}) = \frac{e^{ik_o|\vec{R}-\vec{r}|}}{4\pi|\vec{R}-\vec{r}|} \qquad [m^{-1}] \tag{2.16}$$

$\vec{R} \equiv (R,0,0)$ and $\vec{r}$ =(x,y,z) represent the receiver location and the scattering eddy position from the transmitter taken as the origin of the system. In Fig.2.2 we show the geometry of our problem where only direct and scattered waves arrive at the receiver, the x axis coincides with the direct path and the incident waves to the receiver and to the eddy are spherical.

From (2.14)- (2.15) the log-amplitude and phase of the signal are given as [10]:

$$\chi(\vec{R},t) = \ln\left(\left|E(\vec{R},t)\right| / \left|E_o(\vec{R})\right|\right) = \Re[\psi_1(\vec{R},t)] \qquad [\text{Np}] \qquad (2.17)$$

$$\varphi(\vec{R},t) = \Im[\psi_1(\vec{R},t)] \qquad [\text{rad}] \qquad (2.18)$$

Where $\Re[\psi_1(\vec{R},t)]$ and $\Im[\psi_1(\vec{R},t)]$ are respectively the real and the imaginary part of the complex function $\psi_1(\vec{R},t)$.

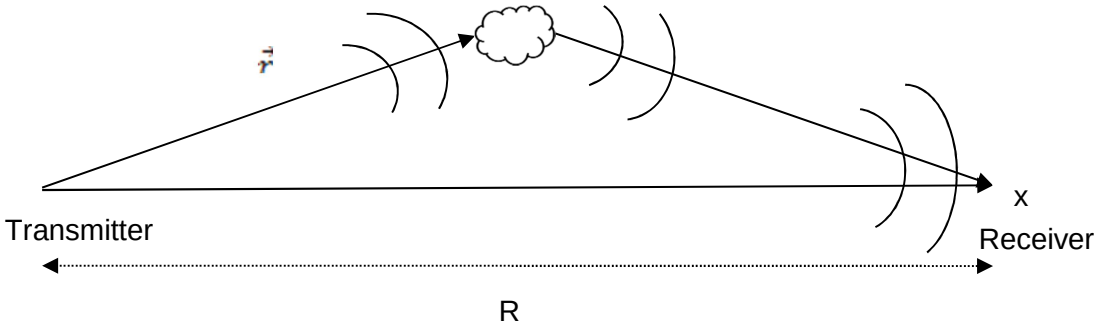

Figure 2. 2:Geometry of the scattering problem for spherical wave. Incident waves to the receiver and to the eddy are spherical. Line-Of-Side is assumed along x-axis.

A point source should generate an electric-field strength that depends only on the scalar distance from transmitter if there are no irregularities in the transmission volume so that for spherical wave propagation electric fields arriving at the turbulence and at the receiver are:

$$E_0(\vec{r}) = \frac{E_0 e^{i\vec{k}\cdot|\vec{r}|}}{|\vec{r}|} \qquad [\text{V/m}] \qquad (2.19)$$

And

$$E_0(\vec{R}) = \frac{E_0 e^{i\vec{k}\cdot R}}{R}. \qquad [\text{V/m}] \qquad (2.20)$$

Following the calculations in Appendix A, we finally we get log-amplitude and phase variances for an incident spherical wave:

$$< \chi^2 >^{3D} = 4\pi^2 k_o^2 \int_0^{\infty} S_{n_1}^{3D}(\kappa)\kappa d\kappa \int_{x_1}^{x_2} \sin^2\left(\frac{x(R-x)\kappa^2}{2Rk_o}\right)dx \qquad [\text{Np}^2] \quad (2.21)$$

$$< \varphi^2 >^{3D} = 4\pi^2 k_o^2 \int_0^{\infty} S_{n_1}^{3D}(\kappa)\kappa d\kappa \int_{x_1}^{x_2} \cos^2\left(\frac{x(R-x)\kappa^2}{2Rk_o}\right)dx \qquad [\text{rad}^2] \quad (2.22)$$

Where x_1 , x_2 are the boundaries of the turbulence, as shown in Fig.2.3. Similar expression were found by Wheelon [11] for slab distribution.

Equation (2.21)-(2.22) can be written in general as:

$$< \chi^2 >^{3D} = 4\pi^2 \Delta x k_o^2 \int_0^{\infty} \kappa S_{n_1}(\kappa) F_{\chi}(\kappa) d\kappa \qquad [\text{Np}^2] \quad (2.23)$$

$$< \varphi^2 >^{3D} = 4\pi^2 \Delta x k_o^2 \int_0^{\infty} \kappa S_{n_1}(\kappa) F_{\varphi}(\kappa) d\kappa \qquad [\text{rad}^2] \quad (2.24)$$

Having defined two functions as:

$$F_{\chi}(\kappa) = \frac{1}{\Delta x} \int_{x_1}^{x_1+\Delta x} \sin^2\left(\frac{x(R-x)\kappa^2}{2Rk_0}\right)dx \quad (2.25)$$

$$F_{\varphi}(\kappa) = \frac{1}{\Delta x} \int_{x_1}^{x_1+\Delta x} \cos^2\left(\frac{x(R-x)\kappa^2}{2Rk_o}\right)dx \quad (2.26)$$

Where $\Delta x = x_2 - x_1$ is the extension of the turbulence in [m]. These are the so called “weighting functions” because, as seen in (2.23)-(2.24), they filter or weight the spectrum shown in the Chapter 1. Therefore it is necessary to analyze them, before proceeding with variances computation. It is done in the following paragraph.

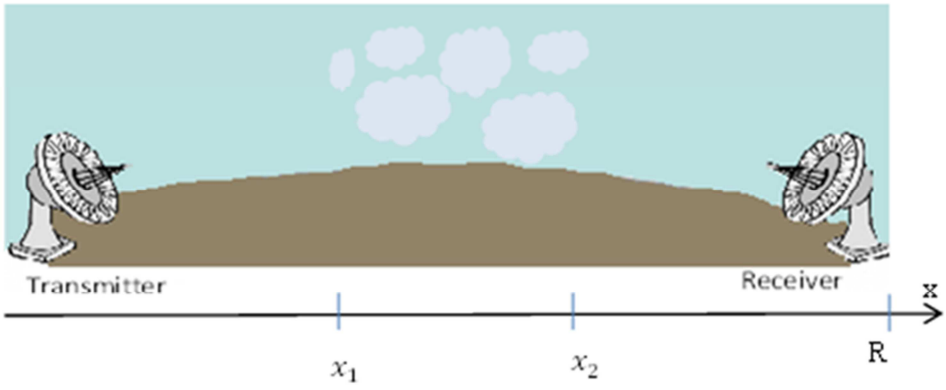

Figure 2. 3: Communication system between two stations with irregularities placed in thick layer in the path, from x1 to x2, distances from the transmitter.

2.1.2 The weighitng functions

As seen in the calculation, functions (2.25)-(2.26) derive from the relation between the direct and the scattered waves, which means they depends on the extension of the perturbation, responsible of the diffractive effects. However, the main dependency relies on the link distance R and the frequency, because their relation with the turbulence indicates if the system works in Fraunhofer of Fresnel regime, defined in (1.11)-(1.12). One can notice that phase and log-amplitude weighting functions (2.25)-(2.26) are complementary. In fact:

$$F_{\chi}(\kappa)+F_{\varphi}(\kappa)=1 \tag{2.27}$$

This is an important property valid for all the configurations (2D/3D) and for all the wave typologies (plane, spherical).

The idea is to solve the integrals finding analytical expressions which describe the behavior of those functions with respect to the variation of the eddy dimensions. Derivations are exposed in Appendix B, obtaining:

$$F_{\chi}(\kappa)=R\frac{1}{4\Delta x}\left\{\frac{2\Delta x}{R}-\sqrt{\frac{2k_0\pi}{\kappa^2 R}}\left\{\left[C\left[\left(1-\frac{2x_1}{R}\right)\sqrt{\frac{\kappa^2 R}{2k_0\pi}}\right]-C\left[\left(1-\frac{2x_2}{R}\right)\sqrt{\frac{\kappa^2 R}{2k_0\pi}}\right]\right]\cos\left(\frac{\kappa^2 R}{4k_0}\right)+\right.\right.$$
$$\left.\left.+\left[S\left[\left(1-\frac{2x_1}{R}\right)\sqrt{\frac{\kappa^2 R}{2k_0\pi}}\right]-S\left[\left(1-\frac{2x_2}{R}\right)\sqrt{\frac{\kappa^2 R}{2k_0\pi}}\right]\right]\sin\left(\frac{\kappa^2 R}{4k_0}\right)\right\}\right\} \tag{2.28}$$

$$F_{\varphi}(\kappa) = R\frac{1}{4\Delta x}\left\{\frac{2\Delta x}{R} + \sqrt{\frac{2k_0\pi}{\kappa^2 R}}\left\{\left[C\left[\left(1-\frac{2x_1}{R}\right)\sqrt{\frac{\kappa^2 R}{2k_0\pi}}\right] - C\left[\left(1-\frac{2x_2}{R}\right)\sqrt{\frac{\kappa^2 R}{2k_0\pi}}\right]\right]\cos\left(\frac{\kappa^2 R}{4k_0}\right) + \right.\right.$$
$$\left.\left. + \left[S\left[\left(1-\frac{2x_1}{R}\right)\sqrt{\frac{\kappa^2 R}{2k_0\pi}}\right] - S\left[\left(1-\frac{2x_2}{R}\right)\sqrt{\frac{\kappa^2 R}{2k_0\pi}}\right]\right]\sin\left(\frac{\kappa^2 R}{4k_0}\right)\right\}\right\} \quad (2.29)$$

Where C(x) and S(x) are *Fresnel integrals*.

There is no need to study the global behavior of these functions because some assumptions can be done according to the regime of work. Hence in the following paragraph, asymptotic formulations for the variances will be derived considering the cuts of (2.28)-(2.29) on the spectrum.

However a simple observation can be done.

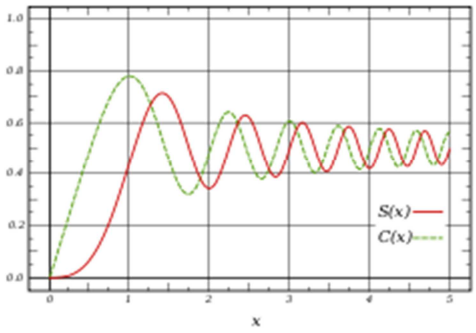

Figure 2. 4: Fresnel integrals. C(x) is the green and S(x) the red line. Both oscillate around 0.5

In Fig.2.5 $x_1 \to 0$ and $x_2 \to R$, we get the formulations of the weighting functions for slab model found by Wheelon [11]. This validates our computations and confirms that the general case is the layer model.

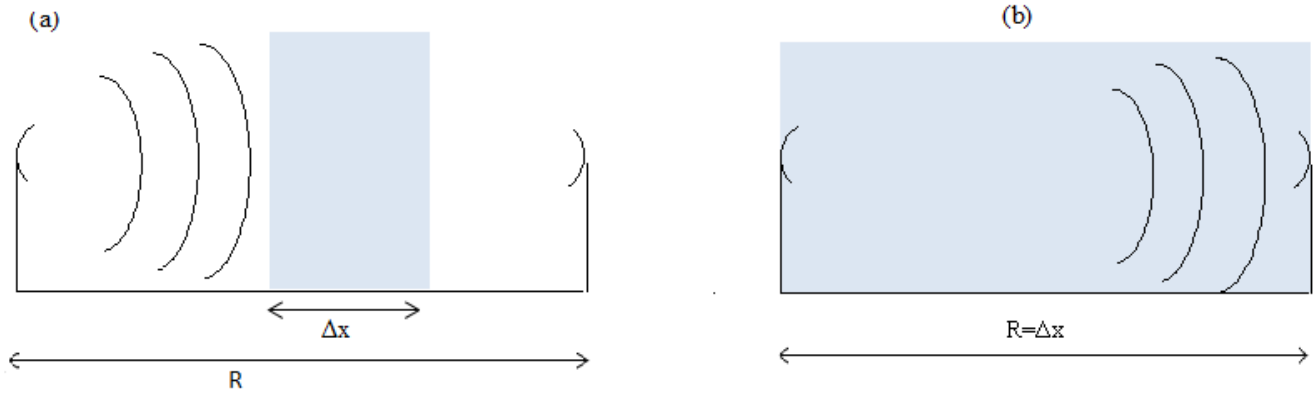

Figure 2. 5: Extending a general layer (a) from transmitter to the receiver, we find the slab model (b). This means slab is only a particular case of the problem even for spherical wave.

2.2 3D Asymptotic formula

At this point we have all the elements to compute the variances: weighting functions and spectrum. They are computed for either Fresnel or Fraunhofer regime, because according to the parameters involved (frequency, path length, layer thickness..), the physical phenomena can change significantly.

2.2.1 Fresnel regime in 3D

Fresnel regime is established for relation (1.11) or in wave-number domain when $\frac{2\pi}{\sqrt{\lambda R}} >> \frac{2\pi}{\mathrm{L_{os}}}$.

Considering the amplitude, this means that highest values of κ , i.e. the smallest eddies, bring the main contribution to scintillation. Consequently, in equation (2.21) we do not consider $S_{n_1}^{3D}\left(\vec{\kappa}\right)$ by Von karman model (1.16) but by the simplified Kolmogorov (1.13), integrating it from 0 to infinity.
Mathematically:

$$\langle \chi^2 \rangle^{3D} = 4\pi^2 {k_0}^2 \Delta x \left[\int_0^{K_{os}} \kappa S_n(\kappa) F_\chi^{layer}(\kappa) d\kappa + \int_{Kos}^{\infty} \kappa S_n(\kappa) F_\chi^{layer}(\kappa) d\kappa \right] \quad . \qquad [\mathrm{Np^2}] \quad (2.30)$$

As function (2.28) is low for the biggest eddies in the 'input range', i.e. before K_{os}, previous relation becomes:

$$\langle \chi^2 \rangle^{3D} = 4\pi^2 {k_0}^2 \Delta x \int_{K_{os}}^{\infty} \kappa S_n(\kappa) F_\chi^{layer}(\kappa) d\kappa = 4\pi^2 {k_0}^2 \Delta x \int_0^{\infty} \kappa S_n'(\kappa) F_\chi^{layer}(\kappa) d\kappa \qquad [\mathrm{Np^2}] \quad (2.31)$$

$S_n'(\kappa)$ and $S_n(\kappa)$ are Kolmogorov and Von Karman spectra respectively.

For phase variance the situation is different, in fact the functions (2.28) start at 1 so that they does not filter the spectrum at low wave-numbers. For this reason we cannot use the Kolmogorov spectrum in the calculations and Von karman model $S_n(\kappa)$ must be applied. Under this assumptions it is possible to drive the analytical derivations.

Rewrite equations (2.21) as:

$$< \chi^2 >^{3D} = 4\pi^2 k_o^2 \int_0^{+\infty} S_{n_1}^{3D}(\kappa) \kappa d\kappa \frac{1}{2} R \int_{\frac{x_1}{R}}^{\frac{x_1+\Delta x}{R}} \left[1 - \cos\left(\frac{\kappa^2 R u (1-u)}{k_0} \right) \right] du \qquad [\mathrm{Np^2}] \quad (2.32)$$

We have already integrated on x obtaining the weighting function, so we could substitute it to the second integral and integrate on κ, but it is analytically hard. Let's solve it on κ before, with Kolmogorov spectrum as already explained.

Making a change of variable $\frac{\kappa^2 R u(1-u)}{k_o} = t$, we find:

$$< \chi^2 >^{3D} = 0.033\pi^2 C_n^2 R^{\frac{11}{6}} k_o^{\frac{7}{6}} \int_0^{+\infty} \frac{1}{t^{\frac{11}{6}}} [1-\cos(t)]dt \int_{\frac{x_1}{R}}^{\frac{x_1+\Delta x}{R}} [u(1-u)]^{\frac{5}{6}} du \qquad \text{[Np²] (2.33)}$$

The first integral is tabulated and it is $\int_0^{\infty} \frac{1}{t^{\frac{11}{6}}} [1-\cos(t)]dt$ =1.728. So log-amplitude variance in fresnel regime is:

$$< \chi^2 >^{3D} = 0.563\ C_n^2 R^{\frac{11}{6}} k_o^{\frac{7}{6}} \int_{\frac{x_1}{R}}^{\frac{x_1+\Delta x}{R}} [u(1-u)]^{\frac{5}{6}} du \qquad \text{[Np²] (2.34)}$$

Where the integral is solved by Hypergeometric functions[1].

Phase variance is more difficult to develop analytically because, as already said, the function (2.28) does not filter small wave-numbers so that Von Karman spectrum is more appropriate than Kolmogorov's. For such a reason it is useful introducing the phase variance for geometrical optics ($k_0 R >> 1$), which has been defined by Wheelon[11]:

$$\langle \varphi_0^{\,2} \rangle = 4\pi^2 \Delta x k_0^2 \int_0^{\infty} \kappa S_n(\kappa, x) d\kappa \qquad \text{[rad²]} \qquad (2.35)$$

Substituting Von karman spectrum we get the expression:

---

[1] In order to enlighten the computation of the integral, we can make another change of variable $\mathbf{u = \frac{1-c}{2}}$; $\mathbf{1-u = 1-\frac{1-c}{2} = \frac{1+c}{2}}$; $\mathbf{c = 1-2u}$

$$\int_{\frac{x_1}{R}}^{\frac{x_1+\Delta x}{R}} [u(1-u)]^{\frac{5}{6}} dx = \frac{1}{4^{\frac{5}{6}}} \int_{1-2\frac{x_1}{R}}^{1-2\frac{x_1+\Delta x}{R}} [1-c^2]^{\frac{5}{6}} dc$$

$$\langle \chi^2 \rangle_{sph} = 0.088\ C_n^2 R^{\frac{11}{6}} k^{\frac{7}{6}} \int_{1-2\frac{x_1}{R}}^{1-2\frac{x_1+\Delta x}{R}} [1-c^2]^{\frac{5}{6}} dc$$

$$\langle \varphi_0^{\,2} \rangle = 0.782\, C_n^2\, \Delta x k_0^2\, K_{os}^{-\frac{5}{3}} \qquad [\text{rad}^2] \qquad (2.36)$$

This is independent of the wave nature, in fact in equation (2.35) there is no weighting function because in geometrical optics diffraction effects are neglected. Observing equation (2.35), (2.21) and (2.22) one can notice that:

$$\langle \varphi^2 \rangle + \langle \chi^2 \rangle = \langle \varphi_0^2 \rangle \qquad [\text{rad}^2] \qquad (2.37)$$

This is a really useful relation linking amplitude and phase, also valid for plane wave. It is really important because it does not depend on the assumption of isotropy and on the paraxial approximation [7]. Obviously it is linked to the property of complementarity (2.27).
Substituting the equation (2.36) and (2.34) in (2.37), phase variance in fresnel regime is:

$$\boxed{\langle \varphi^2 \rangle^{3D} = \langle \varphi_0^2 \rangle \left(1 - 0.72 \left(\frac{RK_{os}^2}{k} \right) \int_{\frac{x_1}{R}}^{\frac{x_1+\Delta x}{R}} [u(1-u)]^{\frac{5}{6}} du \right)} \qquad [\text{rad}^2] \qquad (2.38)$$

As expected phase variance depends on Kos, but amplitude does not.

2.2.2 Fraunhofer regime in 3D

In Fraunhofer configuration, Fresnel distance is greater than Los which means that 'Energy Input Region' (from 0 to K_{os}) has to be considered in wave-numbers domain even for log-amplitude variance. Hence it is necessary using the von Karman spectrum (1.16) for both log-amplitude and phase.
We cannot follow the same approach developed for Fresnel regime because now analytical derivations for variances are too difficult. However, considering the definition of Fraunhofer regime (1.12) and noticing that in (2.28)-(2.29) the coefficient $\sqrt{\frac{2k_0\pi}{\kappa^2 R}}$ actually is the inverse Fresnel number, the two weighting functions tend to 0.5, more rapidly for higher value of Fresnel number.
So it is possible to solve equations (2.21)-(2.22) substituting 0.5 to the weighting functions:

$$\langle \chi^2 \rangle^{3D} = 2\pi^2 k_0^2 \int_0^{\infty} \kappa S_{n_1}(\kappa, x) \Delta x d\kappa \qquad [\text{Np}^2] \qquad (2.39)$$

$$\langle \varphi^2 \rangle^{3D} = 2\pi^2 k_0^2 \int_0^{\infty} \kappa S_{n_1}(\kappa, x) \Delta x d\kappa \qquad [\text{rad}^2] \qquad (2.40)$$

Considering Von Karman spectrum (1.16), we obtain the asymptotic expressions of log-amplitude and phase variances in Fraunhofer regime:

$$\langle \chi^2 \rangle^{3D} = 0.391 \Delta x k^2 C_n^2 K_{os}^{-\frac{5}{3}} \qquad [\text{Np}^2] \qquad (2.41)$$

$$\langle \varphi^2 \rangle^{3D} = 0.391 \Delta x k^2 C_n^2 K_{os}^{-\frac{5}{3}} \qquad [\text{rad}^2] \qquad (2.42)$$

More simply we could have noticed that:

$$\langle \chi^2 \rangle^{3D} = 2\pi^2 \Delta x k_0^2 \int_0^{\infty} \kappa S_n(\kappa, x) d\kappa = \frac{1}{2} \left\langle \varphi_0^2 \right\rangle \qquad [\text{Np}^2] \qquad (2.43)$$

Where $\left\langle \varphi_0^2 \right\rangle$ is the phase for geometrical optics (2.30).

For the phase variance thanks to equation (2.31):

$$\langle \varphi^2 \rangle^{3D} = \left\langle \varphi_0^2 \right\rangle - \left\langle \chi^2 \right\rangle = \frac{1}{2} \left\langle \varphi_0^2 \right\rangle \quad . \qquad [\text{rad}^2] \qquad (2.44)$$

Both functions are independent from the distance transmitter-layer so the variances are always the same whatever the position of layer along the link.

At this point, we have the formulation of the variances and their behaviour according to the relation between the system parameters (frequency, path length) and the irregularities of the medium. All the comments about the formulas will be explained in Chapter 3, together with the comparison to the plane wave approach, commonly used. For the instant we still remain on the analytical formalism, studying the effects on the computation of the variances passing from 3D to 2D.

2.3 Variances definitions for the reduced 2D configuration

The 2D reduction is useful to improve computational time for numerical resolution of the problem but it can introduce some errors in the calculation of the variances. This means the Rytov approximation, Helmholtz equation and the physical scenario are the same as before, so we only

discuss about the changes in the formulas avoiding redundancy repeating points already explained. Main changes concern the Green function and the incident electric fields, now expressed as:

$$G^{2D}(R,\vec{r}) = \frac{i}{4} H_0^1\left[k_0 \left|R-\vec{r}\right|\right] \qquad [m^{-1}] \qquad (2.45)$$

$$E_0(\vec{r}) = \frac{E_0 e^{i\vec{k}\cdot\vec{r}}}{\sqrt{r}} \qquad [V/m] \qquad (2.46)$$

$$E_0(\vec{R}) = \frac{E_0 e^{i\vec{k}\cdot R}}{\sqrt{R}} \qquad [V/m] \qquad (2.47)$$

where $H_0^1[x]$ is the first kind, zero order Hankel function.

Wave equation has to be solved in the vertical plane x-z so that $\vec{k} \equiv (k_x, k_z)$ $\vec{r} \equiv (x,z)$ $n_1(\vec{r},t) \equiv n_1(x,z,t)$.

Assuming high frequency and small scattering angle as usual:

$$k_0\left|R-\vec{r}\right| >> 1 \qquad R - x >> z$$

(2.45) becomes:

$$G^{2D}(R,\vec{r}) \cong \frac{e^{i\frac{\pi}{4}} e^{ik_0(R-x)} e^{ik_0\frac{z^2}{2(R-x)}}}{\sqrt{8\pi k_0 (R-x)}} \qquad [m^{-1}] \qquad (2.48)$$

At this point it is useful considering the system of Fig.A.1 for 3D. The cut involves κ to be projected on the vertical plane x-z, as shown in Fig. 2.6.

As in 3D calculation derived in Appendix A, $\nu = \frac{\pi}{2}$ so the final expressions for log-amplitude and phase variances in two dimensions are:

$$< \chi^2 >^{2D} = 2\pi k_o^2 \int_0^\infty d\kappa S_{n_1}^{3D}(\kappa)\kappa \int_0^{2\pi} d\omega \int_{x_1}^{x_2} \sin^2\left(\frac{x(R-x)(\kappa \sin\omega)^2}{2Rk_o}\right) dx \qquad [\text{Np}^2] \quad (2.49)$$

$$< \varphi^2 >^{2D} = 2\pi k_o^2 \int_0^\infty d\kappa S_{n_1}^{3D}(\kappa)\kappa \int_0^{2\pi} d\omega \int_{x_1}^{x_2} \cos^2\left(\frac{x(R-x)(\kappa \sin\omega)^2}{2Rk_o}\right) dx \qquad [\text{rad}^2] \quad (2.50)$$

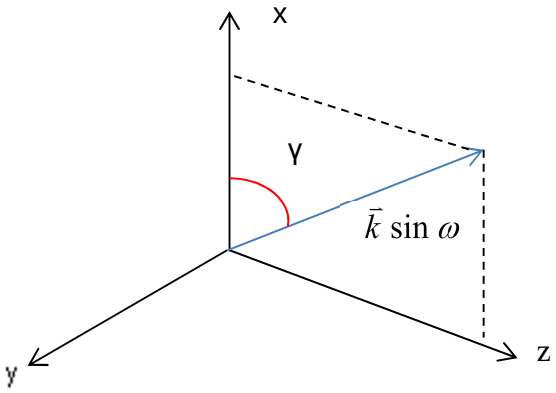

Figure 2. 6: System for 2D geometry. κ in 3D is projected on x-z plane

These are new calculations, never been derived. Recently Fabbro and Feral [19] gave a similar formulation but for plane wave in a slab distribution.

Comparing these expressions with the others of the 3D we notice two points:

- the spectrum is still the same and depends on κ.

- the reduction affects the weighting functions, in fact now they do not vary along a transverse plane but only along an transverse axis with respect to the direction of propagation. Hence the weighting functions are $F(0,\kappa\sin\omega)$. In Fig.2.7 is reported a representation of wavenumber space in 2D, under the consideration of the Appendix A, i.e. $\kappa = k_r$ as $\nu = \frac{\pi}{2}$.

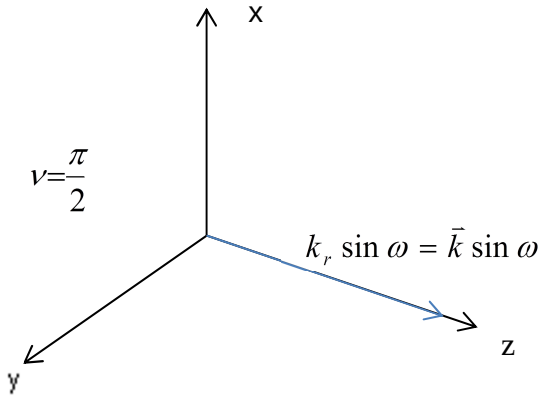

Figure 2.7: As the azimuthal angle $\nu=\frac{\pi}{2}$, wavenumber lies along z, transverse to x .Thus the projection of κ is equal to the projection of k_r

The integration on the angular distance of the wavenumber from the vertical plane represents a 'compression' of the 3D eddies on that plane. This leads to the error explained in the next paragraph.

2.4 2D asymptotic formulas

Now weighting functions depend on the angular distance with respect the transverse axis, so it is not trivial to find a complete formula and anyway we are not even interested in it . For this reason we directly propose the variances in each regimes.

2.4.1 Fresnel regime in 2D

Physical explanation is the same as 3D, so we proceed in the same way considering a kolmogorov model spectrum (1.13) for log-amplitude and Von karman (1.16) for phase variance.
Starting from log-amplitude variance (2.49) and making the variable change x=Ru, we get:

$$<\chi^2>^{2D} = 2\pi k_o^2 \int_0^{+\infty} S_{n_1}^{3D}(\kappa)\kappa d\kappa \int_0^{2\pi} d\omega \frac{1}{2} R \int_{\frac{x_1}{R}}^{\frac{x_1+\Delta x}{R}} \left[1-\cos\left(\frac{(\kappa\sin\omega)^2 Ru(1-u)}{k_0}\right)\right] du \qquad [\text{Np}^2]\ (2.51)$$

Then, considering Kolmogorov spectrum (1.13) and making another change of variable:

$$\frac{Ru(1-u)(\kappa\sin\omega)^2}{k_0} = t$$

we obtain:

$$<\chi^2>^{2D} = 0.033\frac{\pi}{2} C_n^2 R^{\frac{11}{6}} k_o^{\frac{7}{6}} \int_0^{+\infty} \frac{1}{t^{\frac{11}{6}}}[1-\cos(t)]dt \int_0^{2\pi} (\sin\omega)^{\frac{5}{3}} d\omega \int_{\frac{x_1}{R}}^{\frac{x_1+\Delta x}{R}} [u(1-u)]^{\frac{5}{6}} du \qquad [\text{Np}^2]\ (2.52)$$

where $\int_0^{\infty} \frac{1}{t^{\frac{11}{6}}}[1-\cos(t)]dt = 1.728$. So 2D log-amplitude variance in Fresnel regime is:

$$<\chi^2>^{2D} = <\chi^2>_{sph_{fresnel}}^{3D} \frac{1}{2\pi}\int_0^{2\pi} \sin^{\frac{5}{3}}\omega d\omega = \frac{<\chi^2>_{sph_{fresnel}}^{3D}}{1.86} \qquad [\text{Np}^2]\ (2.53)$$

It means that studying a simplified version 2D of the real case 3D we commit an error ~53%, which is not negligible. The same factor was found for slab model in plane wave formalism and tested by Fabbro and Feral [19].
For the phase variance we still use the relation (2.37), obtaining:

$$< \varphi^2 >^{2D} = \langle \varphi_0^2 \rangle \left(1 - 0.387 \left(\frac{RK_{os}^2}{k_0} \right)^{\frac{5}{6}} \int_{\frac{x_1}{R}}^{\frac{x_1+\Delta x}{R}} [u(1-u)]^{\frac{5}{6}} du \right) \quad [\text{rad}^2] \quad (2.54)$$

Where the integral is solved by Hypergeometric functions.

The log-amplitude variance is lower in 2D but the phase is slightly higher than the real 3D, due to the coefficients involved. Anyway this error is negligible so that:

in Fresnel regime, the dimensional reduction has no problem only for the phase variance but for log-amplitude it is necessary to take always into account a correction factor of 1.86.

2.4.2 Fraunhofer regime in 2D

Even for Fraunhofer regime in 2D the weighting functions reach the asymptotic value 0.5, this will lead to same results than for the 3D problem.

$$\langle \chi^2 \rangle^{2D} = 0.391 \Delta x k_0^2 C_n^2 K_{os}^{-\frac{5}{3}} \quad [\text{Np}^2] \quad (2.55)$$

$$\langle \varphi^2 \rangle^{2D} = 0.391 \Delta x k_0^2 C_n^2 K_{os}^{-\frac{5}{3}} \quad [\text{rad}^2] \quad (2.56)$$

This means that:
in Fraunhofer regime, the dimensional reduction has no effect both in log-amplitude and phase so it is allowed without problem.

Thus, the main problem comes when the system works in Fresnel regime because the computation of the log-amplitude in 2D underestimates the real situation in 3D. In the following chapter we analyse this conclusion with other calculations made for plane wave with an eye to the results recently found by Fabbro and Feral [19] for the plane wave for turbulence Slab distributed. In addition, observations to the formulas of this chapter are presented, comparing them in parallel with plane wave approach largely studied by Wheelon[11].

Chapter 3

Comparison between spherical and plane wave approach

In this section comments of the previous Chapter and comparisons with the studies done in literature concerning plane wave are presented. Firstly we examine the differences with the plane wave weighting functions found by Wheelon [11], followed by an analysis of the variances for which a distinction of 2D and 3D is necessary. For this reason the second paragraph has the structure of Chapter 2 for a better comprehension.

3.1 Differences between plane and spherical weighting functions

Authors largely studied scintillation effects by the use of the plane wave, because of the simplicity of the formalism allowed when the observer is far from the source as the plane wavefront well approximates the spherical wavefront locally at long ranges.
It is the classical scenario of the optical astronomy when turbulences in troposphere or ionosphere are very far from the transmitter (star). In this case several phenomena are notable, as the change of apparent position or *quivering* of a star. In addition, the intensity of a stellar signal changes randomly with time. This form of scintillation is called *twinkling* and is observed even on still nights.
For these cases amplitude and phase variances are given by [11]:

$$< \chi^2 >_{plane}^{3D} = 4\pi^2 k_o^2 \int_0^{\infty} S_{n_1}^{3D}(\kappa)\kappa d\kappa \int_{x_1}^{x_2} \sin^2\left(\frac{x\kappa^2}{2k_o}\right) dx \qquad [\mathrm{Np}^2] \quad (3.1)$$

$$< \varphi^2 >_{plane}^{3D} = 4\pi^2 k_o^2 \int_0^{\infty} S_{n_1}^{3D}(\kappa)\kappa d\kappa \int_{x_1}^{x_2} \cos^2\left(\frac{x\kappa^2}{2k_o}\right) dx \qquad [\mathrm{rad}^2] \quad (3.2)$$

With weighting function defined as:

$$F_{\chi}(\kappa) = \frac{1}{\Delta x} \int_{x_1}^{x_2} \sin^2\left(\frac{x\kappa^2}{2k_0}\right) dx \quad (3.3)$$

$$F_{\varphi}(\kappa)=\frac{1}{\Delta x}\int_{x_1}^{x_2}\cos^2\left(\frac{x\kappa^2}{2k_0}\right)dx \tag{3.4}$$

And equal to:

$$F_{\chi\ plane}(\kappa)=\frac{1}{2}\left\{1-\frac{2k_0}{\Delta x\kappa^2}\cos\left[\frac{\kappa^2(R-x_2)}{k_0}\left(1+\frac{\Delta x}{2(R-x_2)}\right)\right]\sin\left(\frac{\Delta x\kappa^2}{2k_0}\right)\right\} \tag{3.5}$$

$$F_{\varphi\ plane}(\kappa)=\frac{1}{2}\left\{1+\frac{2k_0}{\Delta x\kappa^2}\cos\left[\frac{\kappa^2(R-x_2)}{k_0}\left(1+\frac{\Delta x}{2(R-x_2)}\right)\right]\sin\left(\frac{\Delta x\kappa^2}{2k_0}\right)\right\} \tag{3.6}$$

Which are a modified version of the equations found by Wheelon [11] who placed the receiver as the origin of the system, as shown in Fig.3.1. In order to compare them with spherical wave results we adapted the equations to transmitter's side.

As done for spherical wave, extending the layer from the transmitter to the receiver we get:

$$F_{\chi\ plane}^{\ layer}(\kappa)=\frac{1}{2}\left\{1-\frac{\sin\left(\frac{\Delta x\kappa^2}{k_0}\right)}{\frac{\kappa^2\Delta x}{k_0}}\right\} \tag{3.7}$$

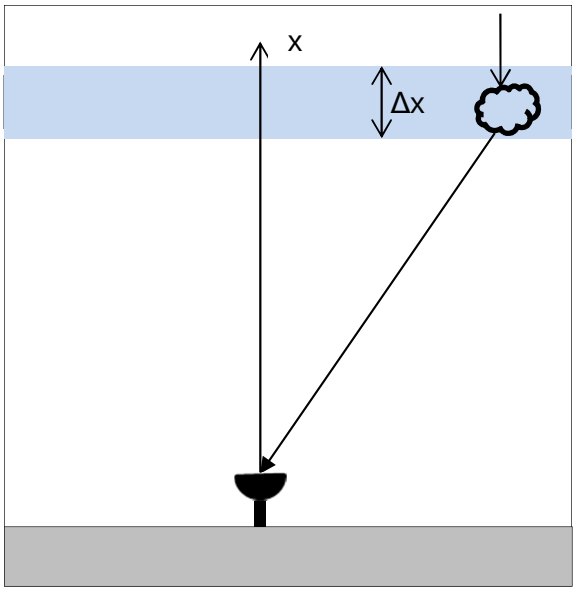

Figure 3. 1: Communication system receiver based

$$F_{\varphi\,plane}^{\;layer}(\kappa)=\frac{1}{2}\left\{1+\frac{\sin\left(\frac{\Delta x\kappa^2}{k_0}\right)}{\frac{\kappa^2\Delta x}{k_0}}\right\} \tag{3.8}$$

Which are the expressions describing the functions for the slab model [11] replacing R with Δx, as show in Fig.3.2.

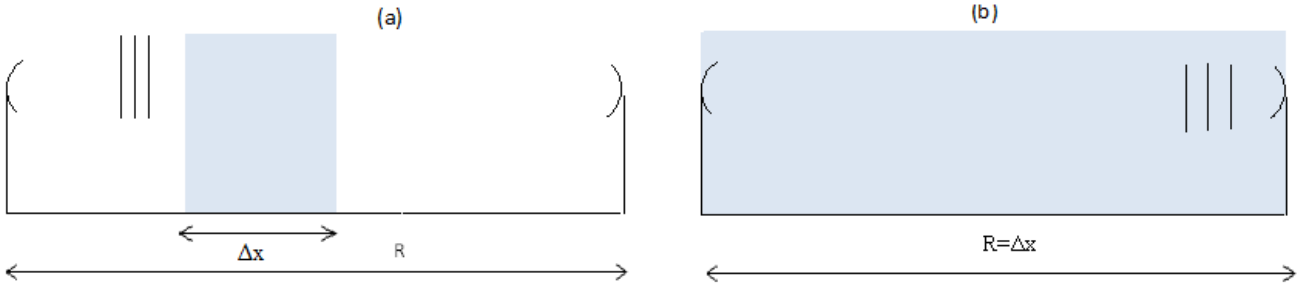

Figure 3. 2: Extending a general layer (a) from transmitter to the receiver, we find the slab model (b) also for plane wave. This means slab is only a particular case of the problem.

As the result is the same as seen in Fig.2.5, we have mathematically proved our assumption:

General case of study is the layer configuration because Slab is only a particular case, independently from the wave typology.

A second comparison between spherical and plane weighting functions can be done, considering the particular case of the turbulence near the receiver.

With some simple steps equations (3.5)-(3.6) are equal again to (3.7)-(3.8) but it is not the same for spherical wave, in fact (2.28)-(2.29) are not equal to the function of spherical slab model [11]. Illustrations in Figg. 3.3 and 3.4:

The reason is that plane wavefront is always the same whatever the distance transmitter-receiver so that for the receiver it doesn't matter if the transmitter is in the same turbulent medium or if it is far from it. In fact the scintillation level depends on the thickness of the layer and on the distance turbulence-receiver (3.5)-(3.6). On the contrary, spherical functions (2.28) and (2.29) depend not only on the layer thickness and the distance turbulence-receiver but also on the distance transmitter-layer. In fact, differently from the plane wave, spherical wavefront is function of the distance.

Thus, the computation of the scintillation can give different results depending on the type of wave considered. A general change concerns the weighting function with respect to the distance involved.

- Dependence on thickness

  Although weighting functions (2.28)-(2.29) and (3.5)-(3.6) are both normalized by Δx, for spherical wave only amplitude of the sinusoids depends on it while for plane wave both amplitude and oscillation frequency do. Consequently for bigger Δx, variation around the asymptote 0.5 gets lower ($1/2 \pm 1/\ \Delta x * (\sin+\cos)$) but on the other hand, oscillation frequency increases only for plane wave weighting function while spherical doesn't change.

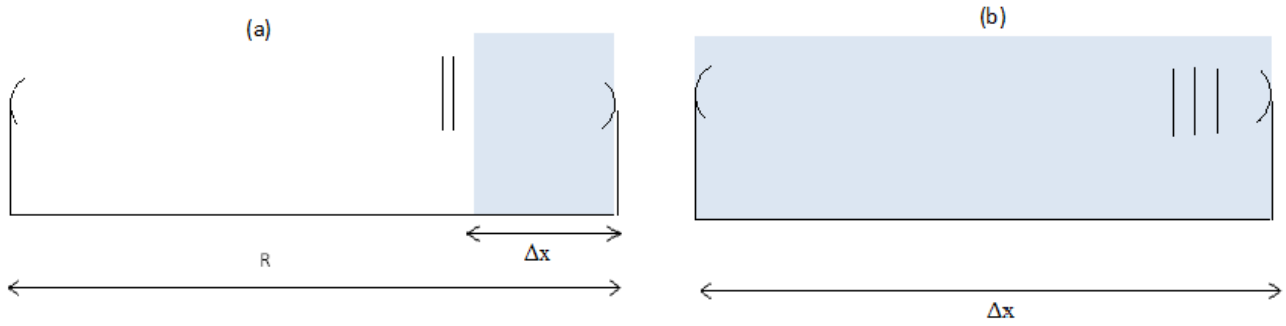

Figure 3. 3: When the irregularities are at the receiver (a), for an incident plane wave an equivalent scenario of a slab with length equal to the thickness of the layer could be assumed (b)

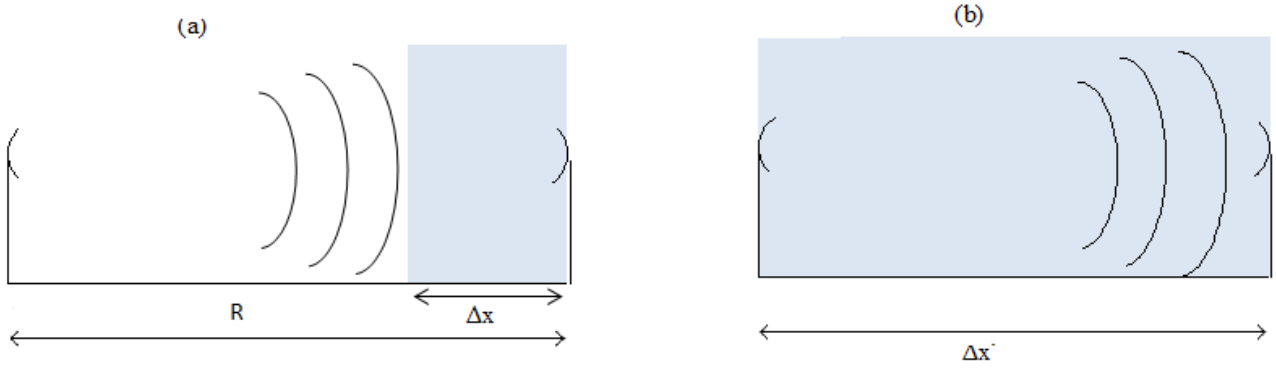

Figure 3. 4: When the irregularities are at the receiver (a), for spherical wave it is not possible to consider an equivalent model of slab with length equal to the thickness of the layer (b.)

- Dependence on R

  First of all, it is useful to remind that R is important because it is related to the Fresnel number. Neither plane nor spherical weighting functions are normalized by R so generally they depend on it, but when layer gets closer to the receiver spherical function still depends on it but the plane one doesn't. This is why, as seen before, plane weighting functions tends to the slab model [11] where $R = \Delta x$, but the spherical has not the same property. In the following paragraph it is shown what happens to the spherical wave in this scenario, studying directly the variances.

3.2 Differences between spherical and plane wave variances

After having analysed the similarities and differences between plane and spherical weighting functions, the consequences on the variances are treated in this paragraph, underlining spherical wave results of chapter 2. Here it is necessary to study separately 3D and 2D for the two regimes.

3.2.1 3D

- Fresnel regime

In Fresnel regime log-amplitude variance for plane wave is given by:

$$\langle \chi^2 \rangle_{plane}^{3D} = 0.307 C_n^2 k_0^{\frac{7}{6}} [(R - x_1)^{\frac{11}{6}} - (R - x_1 - \Delta x)^{\frac{11}{6}}] \quad [\text{Np}^2] \qquad (3.9)$$

Changing again Wheelon result [11] for a transmitter based system. As expected for this regime even the log-amplitude variance for plane wave does not depend on the wave-number and K_{os}.

Consequently, it is possible to analyse the differences between plane and spherical approaches considering a link for different position of the turbulent layer.

The system works at 5GHz frequency for a distance equal to 15km where a 1km turbulent layer is at a position from 0- to 14km from the transmitter. $C_n^2 = 10^{-12} m^{-\frac{2}{3}}$ and $L_{os} = 100 m$ so that Fresnel number is 0.06. In Fig.3.5 the plots of (3.9) and (2.36) versus x1, distance from transmitter to the layer.

This figure illustrates a particular characteristic concerning the wave typology, whatever the distances involved. In the case of the incident spherical wave, reciprocity of the variance appears clearly because of the curve symmetry observed with respect to the mid-distance. In other words an inversion of the transmitter and receiver does not change the result. This is why the peak value is when the layer at the middle of the path. Variance for incident plane wave does not show the same property; in fact it is a decreasing function which leads to a second observation. When the irregularities are close to the source it overestimates the spherical log-amplitude variance with a huge error of 140%, which decreases until the layer is at the receiver's side.

Thus it seems that plane wave is a good approach when the receiver is inside the turbulence but an observation has to be done. In Fig.3.6 a system with the same parameters as before is shown, changing link to 6 km with the 4km turbulent layer on the receiver (2km from transmitter).

Differently from the previous case, there is not a complete convergence because the irregularities are on the receiver's side, but layer covers a big part of link.

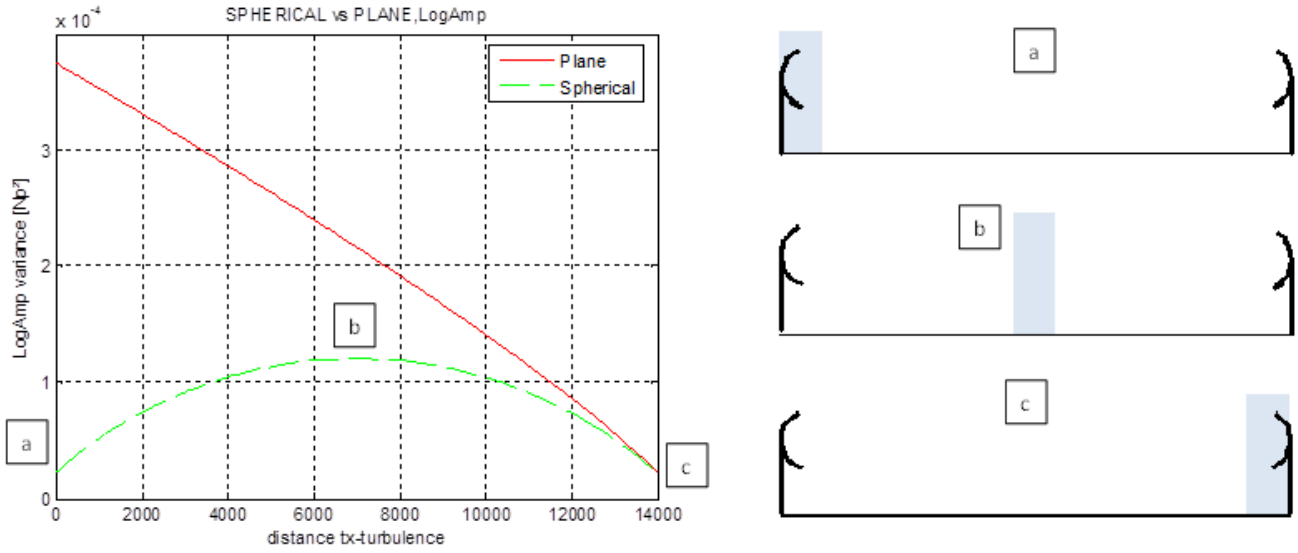

Figure 3. 5:Log-amplitude variances for spherical and plane wave versus x1. Three main cases concern: a)turbulence on the transmitter, b) turbulence in the mid-path, c) turbulence on the receiver

So the overall conclusion is:

The approximation spherical to plane wave gets better when turbulence is far from the transmitter and near the receiver until ratio layer thickness / path length is small, obviously so much better for longest link.

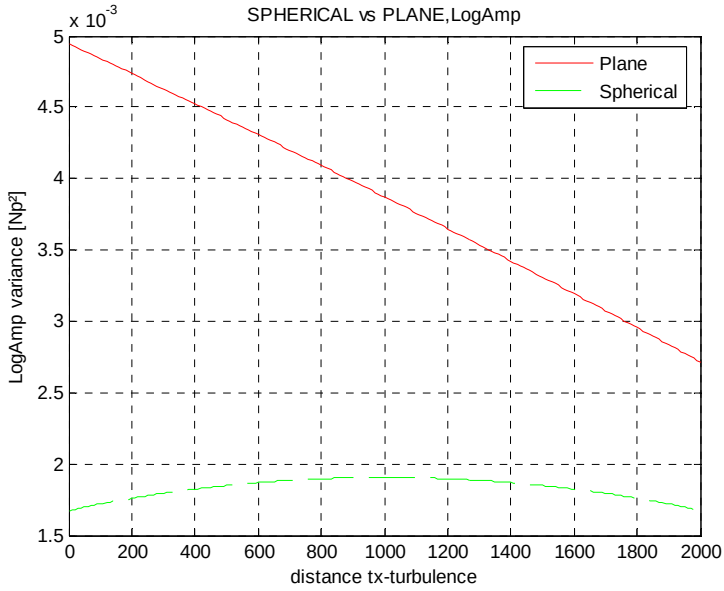

Figure 3. 6: Log-amplitude variances for spherical and plane wave versus x1. This time there is no convergence even when the turbulence is on the receiver, because the layer is too extended.

To have a clear idea of these conclusions, in Fig. 3.7 we plotted Von Karman Spectrum (1.16) multiplied by κ((2.21) and (3.1)), superposed to the plane and spherical log-amplitude weighting functions (3.5) and (2.28). As we are in Fresnel regime, the weighting Functions filter it starting from values greater than K_{os} (yellow vertical line). In this way we are allowed to use the simpler (1.13),

which is the descendant slope of the red curve. This is a graphical explanation for the consideration of par.2.2.1.

The plot is repeated three times, one for each of the main points:

- Layer next to the transmitter. x1=0m
- Layer in the middle of the link. x1=7km.
- Layer next to the receiver. x1=14km

Cyan and green lines are respectively for plane and spherical wave weighting functions while the black one is for their asymptote at 0.5. Red line is the spectrum multiplied by κ and normalized on its maximum value to have a clear representation.

Previous observations are verified here. In Fig. 3.7 (a) and (c) spherical weighting function (green line) is the same, therefore log-amplitude variances are equal. For the plane wave (cyan line) this is the true, in fact in the last figure it is different. It implies reciprocity for spherical but not for plane wave.

Fig.3.7 (a) and (b) illustrate the overestimation of the plane wave: it rises before spherical one so that it takes more contribution from the spectrum, mainly in the first part where there is more energy. For a slab geometry, Wheelon [11] calculated that spherical log-amplitude variance is always 40% less than plane one. In our case the error changes according to the position of the turbulent layer.

Third point to note: in Fig.3.7.b) spherical function rises to 0.5 before than the other figures; this means, when the layer is in middle of the link, the variance is the highest. In our case it is about 5 times greater than first and last case.

Thus we saw that plane and spherical log-amplitude variances in Fresnel regime have the same behaviour with respect to the outer scale, but in general they present some differences.

Now it is useful to analyse the phase to check if the same observations are still valid.

As for spherical wave, phase variance is more difficult to develop analytically so by (2.37) phase variance for plane wave is:

$$\langle \varphi^2 \rangle_{plane}^{3D} = \langle \varphi_0^2 \rangle \{1 - 0.393 (\frac{K_{os}^2}{k})^{\frac{5}{6}} R^{-1} [(R - x_1)^{\frac{11}{6}} - (R - x_1 - \Delta x)^{\frac{11}{6}}]\} \quad [\text{rad}^2] \quad (3.10)$$

As expected even for plane wave phase variance depends on Kos. With the same approach used for log-amplitude, we propose an analysis of the phase variances.

In Fig.3.8 the comparison between spherical and plane phase variances with respect to the position of the layer from the transmitter is shown. Reciprocity can be noted even in the phase because this is a characteristic of the wave. This time, plane wave underestimates the spherical one but always unless the irregularities are near the receiver. Anyway now the error is about 2% so it is negligible. This

effect is linked to the property of complementarity of the phase and log-amplitude weighting functions. For the same reason the minimum appears when the layer is in the middle of the link.

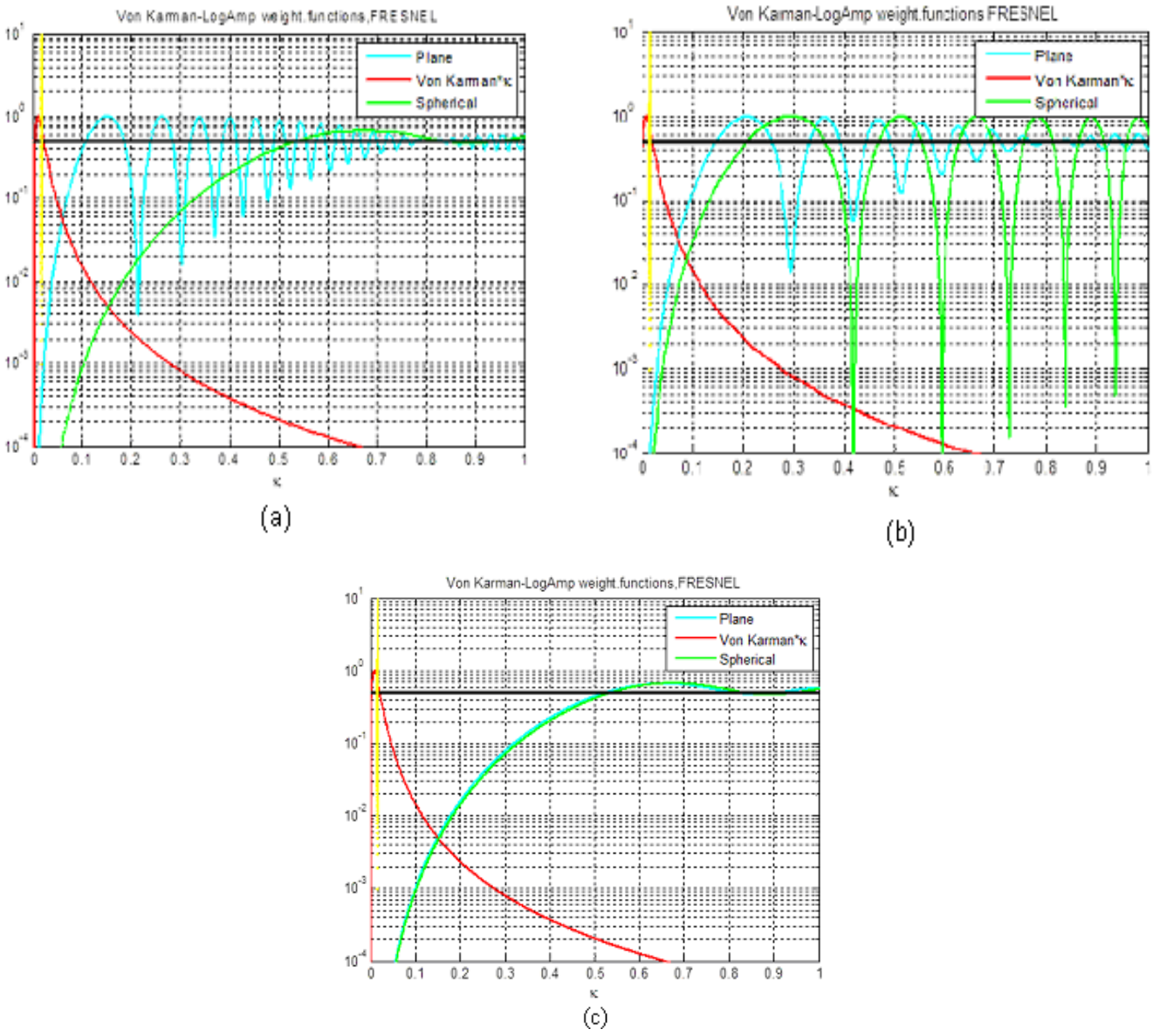

Figure 3. 7: Superposition of spectrum and the log-amplitude weighting functions in Fresnel regime for irregularities near the transmitter (a), in the mid-path (b) and near the receiver (c). In abscissa the value of κ .The spectrum is normalized on its maximum value to have a clear representation

In Fig.3.9 again the plots of the superposition of spectrum and weighting functions for the main three positions in which layer can be. Differently from log-amplitude, now the weighting functions do not filter wavenumbers lower than K_{os} (yellow vertical line) so that we must consider the overall spectrum. This is a graphical explanation for the consideration of par. 2.2.1. Blue and green lines are respectively for plane and spherical wave weighting functions while the black one is for their asymptote at 0.5. Red line is the spectrum multiplied by κ and normalized on its maximum value to have a clear representation.

Reciprocity and approximation plane-spherical wave are clear, let's focus the attention on the different values the phase variance can reach. Logical consequence of what said for Fig. 3.8 and for the log-amplitude, is that when the layer is in middle of the path the phase variance is minima, but an observation is necessary. For all the three cases the function starts at 1 then decreases to 0.5, but it does that when the spectrum has really low energy.

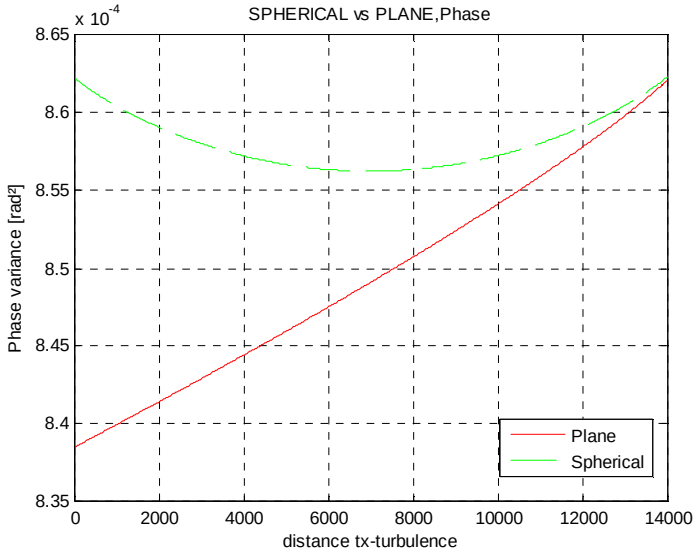

Figure 3. 8: Phase variances for spherical and plane wave versus x1. Thickness is still the same but the turbulence moves towards the receiver

For this reason the phase variance is almost the same whatever the position of the layer along the path. In fact the ratio between the maximum and the minimum of Fig. 3.8 is about 1. It is more precise if the distance R is greater.

In conclusion, in our study concerning the spherical wave, it has been demonstrated that:

in Fresnel regime we expect different log-amplitude but the same phase variance according to the position of the turbulent layer along the link

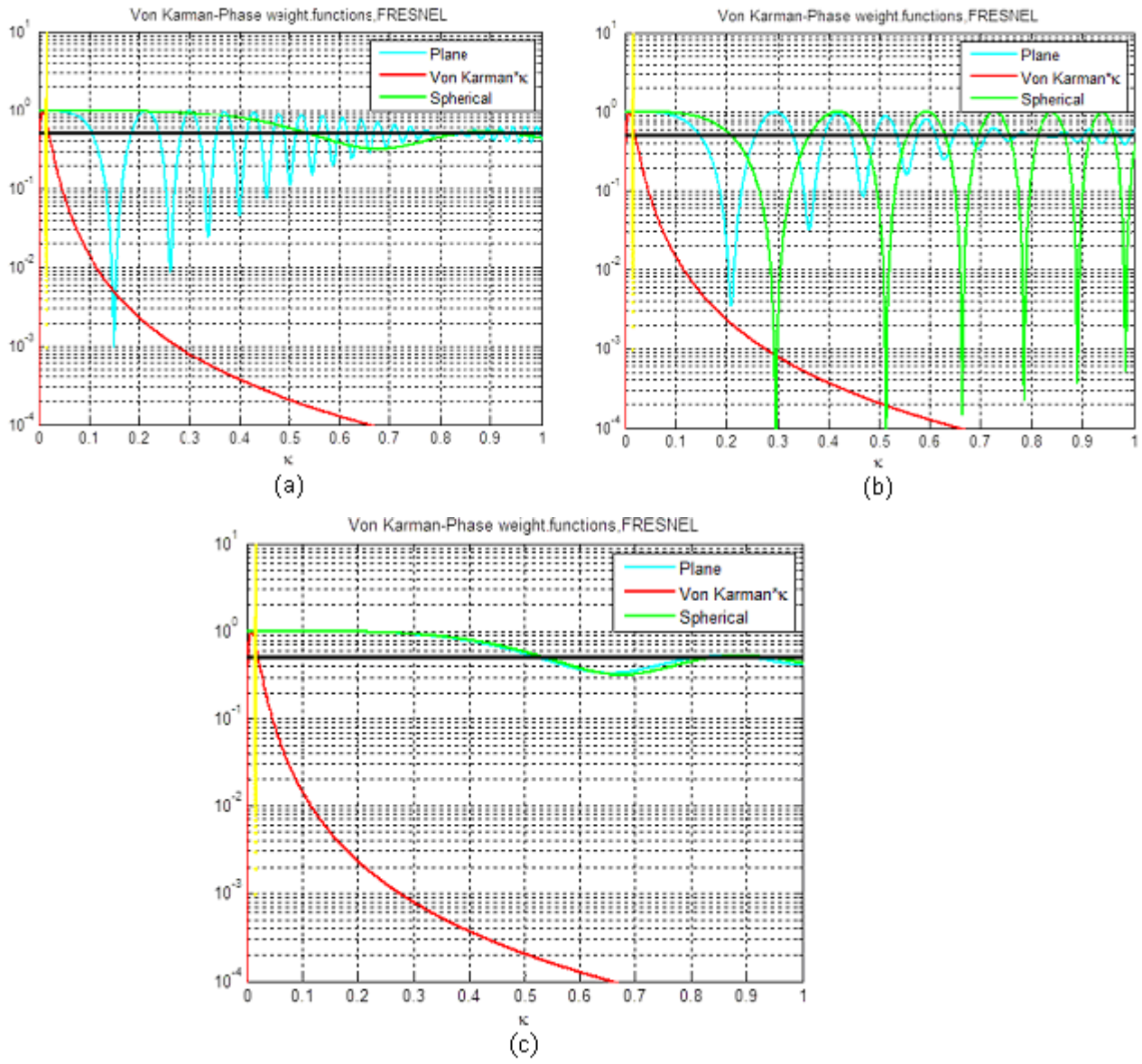

Figure 3. 9: Superposition of spectrum and the phase weighting functions in Fresnel regime for irregularities near the transmitter (a), in the mid-path (b) and near the receiver (c). Spectrum is normalized by its maximum value to have a clear representation.

- **3D Fraunhofer**

Fraunhofer regime is exactly the same as for spherical wave, in fact the weighting functions (3.5)-(3.6) tends to 0.5, more or less rapidly depending on the Fresnel number.

Graphical example is given in Fig.3.10 illustrating the situation of the previous paragraph but changing the Fresnel number to get Fraunhofer regime. Given the same path we modify L_{os} down to 1m and the frequency up to 30GHz, so that Fresnel number is equal to 12.24. Turbulent layer is at 9km from the transmitter.

The first crossing of the asymptote (black line) is reached by the weighting functions for $\kappa << K_{os}$ (yellow line), as expected. This means that, differently from Fresnel regime, weighting functions don't filter the values of small wave-numbers, so even the biggest eddies influence the log-amplitude variance. After crossed the value 0.5, the functions oscillate and at K_{os} they are almost constant.

Under this observation, log-amplitude and phase variance for Fraunhofer regime are equal to the spherical ones:

$$\langle \chi^2 \rangle_{plane}^{3D} = \langle \chi^2 \rangle_{sph}^{3D} \tag{3.11}$$

$$\langle \varphi^2 \rangle_{plane}^{3D} = \langle \varphi^2 \rangle_{sph}^{3D} \tag{3.12}$$

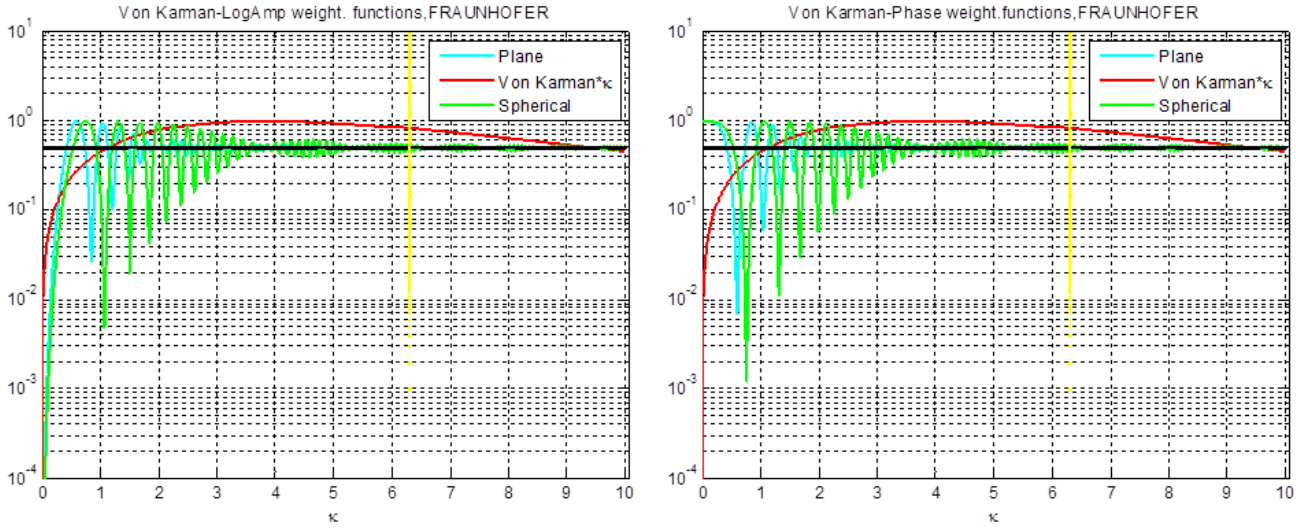

Figure 3. 10 *Superposition of spectrum and the log-amplitude (left) and phase (right) weighting functions with respect to κ, in Fraunhofer regime. Spectrum is normalized on its maximum value to have a clear representation.*

Consequently:

in Fraunhofer regime, variances are independent of the turbulent layer position and of the wave typology, differently from Fresnel regime.

Now we have an overall view of the 3D, where the scintillation level can be differently quantified regarding not only the relation among frequency, path length and turbulence (Fresnel number) as explained in the chapter 2, but also the wave typology. In fact we demonstrated that there are some conditions to the use of plane wave.

In the following paragraph, we examine the 2D to check if the conclusions are the same.

3.2.2 2D

The dimensional reduction in the spherical wave led to a big error for the Fresnel regime and convergence with the 3D for Fraunhofer regime. The task of this paragraph is to control if something changes when a plane wave is considered.
Considering (3.1)-(3.2) and the observations of par.2.3, 2D variances for plane wave are defined as:

$$\langle \chi^2 \rangle_{plane}^{2D} = 2\pi k_0^2 \int_0^{\infty} d\kappa S_{n_1}^{3D}(\kappa)\kappa \int_0^{2\pi} d\omega \int_{x_1}^{x_1+\Delta x} \sin^2\left(\frac{(\kappa \sin\omega)^2 x}{2k_0}\right) dx \quad [\text{Np}^2] \quad (3.13)$$

$$\langle \varphi^2 \rangle_{plane}^{2D} = 2\pi k_0^2 \int_0^{\infty} d\kappa S_{n_1}^{3D}(\kappa)\kappa \int_0^{2\pi} d\omega \int_{x_1}^{x_1+\Delta x} \cos^2\left(\frac{(\kappa \sin\omega)^2 x}{2k_0}\right) dx \quad [\text{rad}^2] \quad (3.14)$$

Which have the same dependency on the angle was the spherical wave. Let's see Fresnel regime first.

- **2D Fresnel**

With the usual consideration and following the steps to get (2.53)-(2.54), we obtain the asymptotic 2D variances for Fresnel regime as:

$$< \chi^2 >_{plane_{fresnel}}^{2D} = < \chi^2 >_{plane_{fresnel}}^{3D} \frac{1}{2\pi} \int_0^{2\pi} d\omega \sin^{\frac{5}{3}} \omega = \frac{< \chi^2 >_{plane_{fresnel}}^{3D}}{1.86} \quad [\text{Np}^2] \quad (3.15)$$

$$< \varphi^2 >_{plane_{fresnel}}^{2D} = \langle \varphi_0^2 \rangle \left(1 - 0.210 \left(\frac{K_{os}^2}{k_0}\right)^{\frac{5}{6}} R^{-1}[(R - x_1)^{\frac{11}{6}} - (R - x_1 - \Delta x)^{\frac{11}{6}}]\right) \quad [\text{rad}^2] \quad (3.16)$$

In (3.15) we find the factor 1.86 equal for our study of an incident spherical wave to a turbulent layer and equal to the study conducted by Fabbro and Feral [19] about an incident plane wave in a slab model. Also the phase is slightly higher than the real 3D as in spherical wave. It leads to a general conclusion:

in Fresnel regime, the dimensional reduction has no problem only for the phase variance but for log-amplitude it is necessary to take always into account a correction factor of 1.86, whatever the wave considered.

- **Fraunhofer regime**

As expected, once again the weighing function tends rapidly to 0.5 so the variances are still the same:

$$\langle \chi^2 \rangle_{plane}^{2D} = \langle \chi^2 \rangle_{plane}^{3D} = \langle \chi^2 \rangle_{sph}^{3D} \tag{3.17}$$

$$\langle \varphi^2 \rangle_{plane}^{2D} = \langle \varphi^2 \rangle_{plane}^{3D} = \langle \varphi^2 \rangle_{sph}^{3D} \tag{3.18}$$

Considering the overall 2D in both regimes, we get two important results:

1. *Dimensional reduction is independent of the wave typology and distribution of irregularities (slab, layer).*

2. *In Fraunhofer regime the variances have the same value for every wave typology, distribution of irregularities and spatial configuration, while in Fresnel regime only the phase has a negligible error varying one of these characteristics but the log-amplitude gets different values.*

In fact, as said in the first chapter, what really matters is the geometry because the real scenario is still the same.

After these two chapters in which the attention has been focused on the analytical formalism, in the next part we implement our numerical model to check if our discussion is valid.

Chapter 4

Numerical model

In the previous two chapters we largely dealt with the 3D and 2D analytical formulations of the scintillation regarding log-amplitude and phase variances for spherical wave (Chapter 2) and comparing them to plane wave formalism (Chapter 3). The limit of the derivations is that they are only valid for weak scattering. For this reason we want to implement a numerical model valid whatever the scattering condition. To do that, the starting point is from the Helmholtz equation in spherical coordinates under parabolic approximation, over which the Split-Step Fourier algorithm (SSF) is based. It allows considering separately refractive and diffractive effects, modeling the whole turbulent layer into a series of sub-layers in which the first effect is gathered into thin screens called Multiple Phase Screen (MPS).

In this context, using a 2D-MPS resolution for the 3D configuration is computationally hard, thus it is clear the use of the dimensional reduction.

4.1 3D numerical resolution

As the Helmholtz equation is the same, it is possible to work on Electric or Magnetic field so we define a general field $\Psi(r) = \Psi$.

Under the condition of chapter 2, therefore the general random wave equation (2.9) becomes:

$$\nabla^2 \Psi + k_0 n^2 \Psi = 0 \tag{4.1}$$

Where ∇^2 denotes the Laplace operator which, in spherical coordinates, is:

$$\nabla^2 = \frac{1}{r^2}\frac{\partial}{\partial r}\left[r^2 \frac{\partial}{\partial r}\right] + \frac{1}{r^2 \sin\theta}\frac{\partial}{\partial \theta}\left[\sin\theta \frac{\partial}{\partial \theta}\right] + \frac{1}{r^2 \sin\theta}\frac{\partial^2}{\partial \varphi^2} \tag{4.2}$$

Considering paraxial approximation, i.e. the angle with respect to the direction of propagation r really small $\theta \to \frac{\pi}{2}$ so that the transverse Laplacian reduces to:

$$\nabla_T^2 = \frac{\partial^2}{\partial\theta^2} + \frac{\partial^2}{\partial\varphi^2} \tag{4.3}$$

we have:

$$\nabla^2\Psi = \frac{1}{r^2}\frac{\partial}{\partial r}\left[r^2\frac{\partial\Psi}{\partial r}\right] + \frac{1}{r^2}\frac{\partial^2\Psi}{\partial\theta^2} + \frac{1}{r^2}\frac{\partial^2\Psi}{\partial\varphi^2} \tag{4.4}$$

$$\nabla^2\Psi = \frac{1}{r^2}\frac{\partial}{\partial r}\left[r^2\frac{\partial\Psi}{\partial r}\right] + \frac{1}{r^2}\nabla_T^2\Psi \tag{4.5}$$

Once we have defined the equation in our reference system, let's find a solution using the reduced field u:

$$u = \frac{\Psi}{\frac{e^{ikr}}{r}} \tag{4.6}$$

where $\Psi(r,\theta,\varphi)$ and $u(r,\theta,\varphi)$. Considering that:

$$\nabla_T^2\Psi = \frac{e^{ikr}}{r}\nabla_T^2 u \tag{4.7}$$

We find the solution:

$$\frac{e^{ikr}}{r}\left[\frac{\partial^2 u}{\partial r^2} + 2\frac{\partial u}{\partial r}ik_0 - {k_0}^2 u\right] + \frac{e^{ikr}}{r}\frac{1}{r^2}\nabla_T^2 u + {k_0}^2 n^2\frac{e^{ikr}}{r}u = 0 \tag{4.8}$$

Using parabolic approximation we can consider only the transverse Laplacian instead of the whole one, because of small variations are supposed near propagation axis ($\frac{\partial^2 u}{\partial x^2} << \frac{\partial u}{\partial x}$ and $\frac{\partial^2 u}{\partial x^2} << \frac{\partial^2 u}{\partial z^2}$) .The standard parabolic wave equation has the disadvantage of being limited to propagation in weakly inhomogeneous media at small angles with a preferred direction. This limitation may be overcome by expressing the parabolic equation in ray coordinates, neglecting the longitudinal diffusion along the rays. Different techniques to treat wider angles have been studied [20].

Thus, neglecting the second derivative with respect to r, (4.8) reduces to:

$$2\frac{\partial u}{\partial r}ik + \frac{1}{r^2}\nabla_T^2 u + k_0{}^2(n^2-1)u = 0 \tag{4.9}$$

And applying the Laplacian transverse (4.3) in (4.9), we obtain:

$$\frac{\partial u(r,\theta,\varphi)}{\partial r} = \frac{i}{2k_0 r^2}\frac{\partial^2 u(r,\theta,\varphi)}{\partial \theta^2} + \frac{i}{2k_0 r^2}\frac{\partial^2 u(r,\theta,\varphi)}{\partial \varphi^2} + \frac{ik_0}{2}(n^2-1)u(r,\theta,\varphi) \tag{4.10}$$

Defining the 2D Fourier Transform of *u* with respect to the transverse plane, in this case angular $\theta - \varphi$:

$$\boxed{U(r,k_\theta,k_\varphi) = FT\{u(r,\theta,\varphi)\} = \frac{1}{(2\pi)^2}\int_{-\infty}^{+\infty}\int_{-\infty}^{+\infty} u(r,\theta,\varphi)e^{-i(k_\theta\theta + k_\varphi\varphi)}d\theta\, d\varphi} \tag{4.11}$$

We obtain a simple differential equation depending on r:

$$\frac{\partial U(r,k_\theta,k_\varphi)}{\partial r} = -\frac{ik_\theta^2}{2k_0 r^2}U(r,k_\theta,k_\varphi) - \frac{ik_\varphi^2}{2k_0 r^2}U(r,k_\theta,k_\varphi) + \frac{ik_0}{2}(n^2-1)U(r,k_\theta,k_\varphi) \tag{4.12}$$

Which gives the solution:

$$U(r,k_\theta,k_\varphi) = e^{ik_0\frac{(n^2-1)}{2}\Delta r}e^{-\frac{i}{2k_0}\left(\frac{1}{r_0}-\frac{1}{r}\right)\left(k_\theta^2+k_\varphi^2\right)}U(r_0,k_\theta,k_\varphi) \tag{4.13}$$

Coming back to space domain:

$$u(r,\theta,\varphi) = e^{ik_0\frac{(n^2-1)}{2}\Delta r}FT^{-1}\left\{e^{-\frac{i}{2k_0}\left(\frac{1}{r_0}-\frac{1}{r}\right)\left(k_\theta^2+k_\varphi^2\right)}FT\{u(r_0,\theta,\varphi)\}\right\} \tag{4.14}$$

For relation (2.10), the term $\frac{(n^2-1)}{2} = n_1$ and the change of phase due to the turbulence can be generally written as:

$$\phi(\theta,\varphi,t) = k_0\int_{r_0}^{r_0+\Delta r} n_1(\xi,\theta,\varphi,t)\,d\xi \qquad \text{[rad]} \tag{4.15}$$

Such that equation (4.14) becomes:

$$u(r,\theta,\varphi) = e^{i\phi(\theta,\varphi,t)} FT^{-1}\left\{ e^{-\frac{i}{2k_0}\left(\frac{1}{r_0}-\frac{1}{r}\right)\left(k_\theta^2 + k_\varphi^2\right)} FT\left\{u(r_0,\theta,\varphi)\right\}\right\} \quad (4.16)$$

Which can be compared with solution found in [21] [22]. Experiments for spherical but mostly incident Gaussian beam have been conducted in [23] [24] [25]. In fact it is similar to a spherical wavefront close.

to propagation axis for narrow angles.

(4.16) shows the Split –Step algorithm:

thanks to 2D Fourier Transform, we manage to divide the problem studying separately refractive and diffractive effects. The second exponential term describes the free-space propagation between two consecutive screens depending on the square modulus of the wavenumber κ, while the first exponential expresses the refractive effect affecting the phase, due to the change of n depending on the turbulent medium. In Fig.4.1 a scheme of the model is proposed.

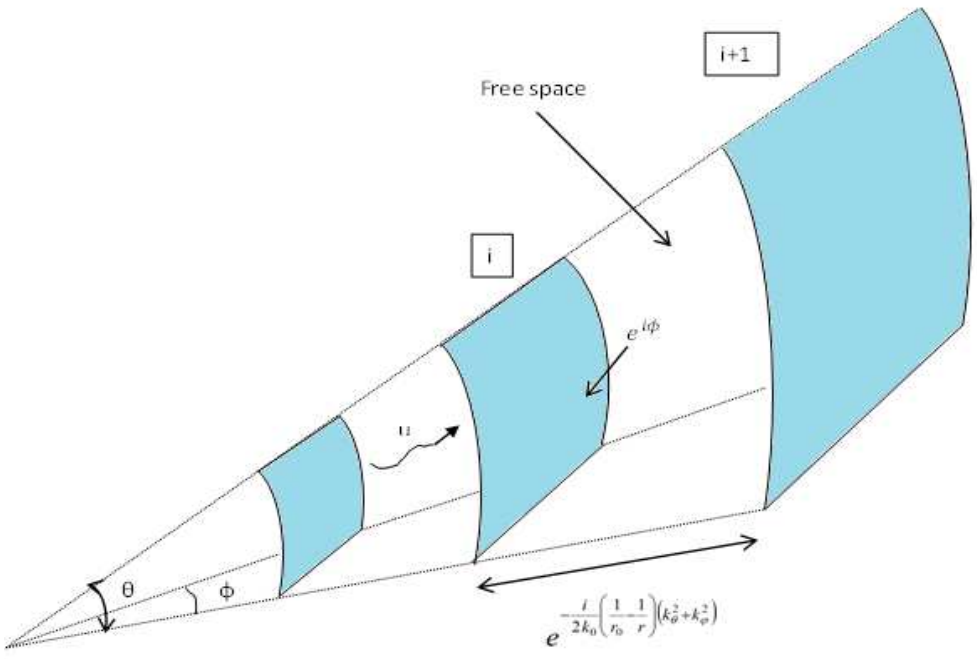

Figure 4. 1: Scheme of the 3D model, 2D Multiple Phase Screen (3D PWE/2D MPS). Wave propagates in free space between two consecutive screens then its phase is modified by i-th screen

- **Screens effect**

In this model the reduced field propagates through a turbulent medium where the effects of the irregularities are expressed by the first exponential. In this way the turbulent layer is divided into sub-layers, with thickness Δr, whose inohomogeneities are compressed in thin screens perpendicular to the propagation axis.

Considering i-th screen, we can write the relation between u^- and u^+, respectively the field before and after the screen, as:

$$u_i^+(r,\theta,\varphi) = e^{i\phi_i(\theta,\varphi,t)} u_i^-(r,\theta,\varphi) \tag{4.17}$$

Where ϕ_i is the value of the phase changed by i-th screen. The phase screen realizations are obtained by sampling a phase distribution whose statistical properties match the spectrum imparted by the medium as explained in the last paragraph.

.

- **Free Space**

Between two screens, *u* moves in free-space but we must pay attention on the effect of this scheme: it is not a classical free-space propagation because also the amplitude varies (in addition to the factor 1/r of the spherical wave). Once the wave is out of the screen there is a mutual interference in the wavefront.

- **Relation between refractive index and phase spectra**

Due to (4.15), phase screen spectrum is related to the spectrum presented in chapter 1. We want to find this relation, which is fundamental for the iterative resolution scheme 3D PWE/ 2D MPS. Indeed, it defines the 2D transverse phase spectrum that must be considered to generate random phase screen $\phi(\theta,\varphi,t)$, as seen in the last paragraph.

Recalling that $<n_1(\vec{r},t)>=0$, it follows that $\phi(\theta,\varphi,t)$ is a centred 2D random variable whose 2D spatial covariance function $B_\phi^{2D}(\breve{y},\breve{z}) = <\phi(\breve{y}',\breve{z}',t)\phi(\breve{y}+\breve{y}',\breve{z}+\breve{z}',t)>$ is given by:

$$B_\phi^{2D}(\breve{y},\breve{z}) = k_0^2 \int_{r_o}^{r_o+\delta r} dr_1 \int_{r_o}^{r_o+\delta r} dr_2 < n_1(r_1,\breve{y}',\breve{z}',t) n_1(r_2,\breve{y}+\breve{y}',\breve{z}+\breve{z}',t) >= k_0^2 \int_0^{+\delta r} dr_1 \int_0^{+\delta r} dr_2 B_{n_1}^{3D}(r_2-r_1,\breve{y},\breve{z}). \tag{4.18}$$

Which is expressed with respect to the distances illustrated in Fig.4.3 where:

$$\breve{y} = r\theta \tag{4.19}$$

$$\breve{z} = r\varphi \tag{4.20}$$

Changing the integration variable to difference $w=r_2 - r_1$ and sum $2r=r_2 + r_1$, equation (4.18) can be rewritten:

$$B_{\phi}^{2D}(\breve{y},\breve{z}) = k_0^2 \int_{-\Delta r}^{+\Delta r} dw \int_{|w|/2}^{\Delta r-|w|/2} dr B_{n_1}^{3D}(w,\breve{y},\breve{z}) = k_0^2 \Delta r \int_{-\Delta r}^{+\Delta r} \left(1-\frac{|w|}{\Delta r}\right) B_{n_1}^{3D}(w,\breve{y},\breve{z}) dw \tag{4.21}$$

If Δr is large with respect to the correlation distance of the turbulent refractive index, the integration can be extended to infinity so that:

$$B_{\phi}^{2D}(\breve{y},\breve{z}) \approx k_0^2 \Delta r \int_{-\infty}^{+\infty} B_{n_1}^{3D}(w,\breve{y},\breve{z}) dw \tag{4.22}$$

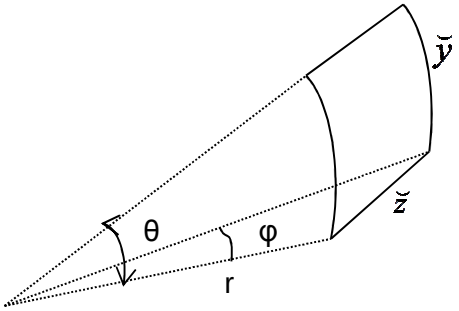

Figure 4. 2: Transversal plane defined by the curvilinear axes on which the covariance function depends

By 2D Fourier Transform we get the definition of phase spectrum:

$$S_{\phi}^{2D}(k_\theta,k_\varphi) = k_0^2 \frac{1}{(2\pi)^2} \int_{-\infty}^{+\infty}\int_{-\infty}^{+\infty} d\theta\, d\varphi\, e^{-i(k_\theta\theta+k_\varphi\varphi)} B_{\phi}^{2D}(w,r\theta,r\varphi) \tag{4.23}$$

Substituting (4.22) in (4.23):

$$S_{\phi}^{2D}(k_\theta,k_\varphi) = \frac{k_0^2\Delta r}{(2\pi)^2} \int_{-\infty}^{+\infty}\int_{-\infty}^{+\infty} d\theta\, d\varphi\, e^{-i(k_\theta\theta+k_\varphi\varphi)} \int_{-\infty}^{+\infty} B_{n_1}^{3D}(w,r\theta,r\varphi) dw \tag{4.24}$$

With parameters of dual domain $k_\theta = \frac{2\pi}{\theta}$ and $k_\varphi = \frac{2\pi}{\varphi}$, angular wavenumbers with respect to θ and

φ . Expressing (4.24) according to the curvilinear axes (3.28)-(3.29), the integral reduces to:

$$S_{\phi}^{2D}(k_{\theta},k_{\varphi})=\frac{k_0^2\Delta r}{(2\pi)^2}\int_{-\infty}^{+\infty}\int_{-\infty}^{+\infty}\frac{d\breve{y}}{w}\frac{d\breve{z}}{w}e^{-i(\frac{k_{\theta}}{w}\breve{y}+\frac{k_{\varphi}}{w}\breve{z})}\int_{-\infty}^{+\infty}B_{n_1}^{3D}(w,\breve{y},\breve{z})dw \tag{4.25}$$

If Δr is large with respect to the correlation distance of the turbulent refractive index we get [22]:

$$\boxed{S_{\phi}^{2D}(k_{\theta},k_{\varphi})=2\pi k_0^2\Delta r\frac{S_{n_1}^{3D}(k_r=0,\frac{k_{\theta}}{r},\frac{k_{\varphi}}{r})}{r^2}} \tag{4.26}$$

k_r and $\sqrt{\left(\frac{k_{\theta}}{r}\right)^2+\left(\frac{k_{\varphi}}{r}\right)^2}$ are respectively the wavenumber k_x along the direction of propagation and modulus κ of the transverse wavenumber $\vec{\kappa}$ considered so far. For $S_{n_1}^{3D}(k_r=0,\frac{k_{\theta}}{r},\frac{k_{\varphi}}{r})$ we consider Von karman spectrum (1.16). This is fundamental for the iterative resolution scheme 3D parabolic/2D phase screens. Indeed, it defines the 2D transverse spectrum $S_{\phi}^{2D}(k_{\theta},k_{\varphi})$ that must be considered to generate random phase screen $\phi(\theta,\varphi,t)$, as seen later in the last paragraph. Successive realizations of $\phi(\theta,\varphi,t)$ are then introduced iteratively in the « Split-Step » resolution written in equation (4.16). The numerical resolution scheme defined in that way is thus a 3D-PWE/2D-MPS (3D-Parabolic Wave Equation/2D-Multiple Phase Screen) iterative scheme.

4.2 2D numerical resolution

Hereby we derive similarly the model for 2D configuration, keeping in mind that the variation now is only in the vertical plane described by r and θ.

Helmholtz equation is still (4.1), but in this case Laplacian term is:

$$\begin{aligned}\nabla^2\Psi&=\frac{1}{r^2}\frac{\partial}{\partial r}[r^2\frac{\partial\Psi}{\partial r}]+\frac{1}{r^2}\frac{\partial^2\Psi}{\partial\theta^2}\\ \nabla^2\Psi&=\frac{1}{r^2}\frac{\partial}{\partial r}[r^2\frac{\partial\Psi}{\partial r}]+\frac{1}{r^2}\nabla_T^2\Psi\end{aligned} \tag{4.27}$$

where is $\nabla_T^2=\frac{\partial^2}{\partial\theta^2}$ the Transverse Laplacian in polar coordinates.

After defining the equation in our reference system, let's find a solution using the reduced field u:

$$u = \frac{\Psi}{\frac{e^{ikr}}{\sqrt{r}}} \tag{4.28}$$

where $\Psi = \Psi(r,\theta)$ and $u = u(r,\theta)$. The transverse Laplacian of u and Ψ are related as:

$$\nabla_T^2 \Psi = \frac{e^{ikr}}{\sqrt{r}} \nabla_T^2 u \tag{4.29}$$

so that (3.36) becomes:

$$\frac{e^{ikr}}{\sqrt{r}}\left[\frac{\partial^2 u}{\partial r^2} + 2\frac{\partial u}{\partial r} ik_0 - {k_0}^2 u\right] + \frac{e^{ikr}}{\sqrt{r}} \frac{1}{r^2} \nabla_T^2 u + {k_0}^2 n^2 \frac{e^{ikr}}{\sqrt{r}} u = 0 \tag{4.30}$$

Neglecting the second derivative with respect to r:

$$2\frac{\partial u}{\partial r} ik + \frac{1}{r^2} \nabla_T^2 u + {k_0}^2 (n^2 - 1) u = 0 \tag{4.31}$$

and applying the Fourier Transform with respect to the transverse coordinate θ, we obtain a simple differential equation depending on r:

$$\frac{\partial U(r,k_\theta)}{\partial r} = -\frac{ik_\theta^2}{2k_0 r^2} U(r,k_\theta,k_\varphi) + \frac{ik_0}{2}\left(n^2 - 1\right) U(r,k_\theta) \tag{4.32}$$

It gives the solution:

$$U(r,k_\theta) = e^{ik_0 \frac{\left(n^2-1\right)}{2}\Delta r} e^{-\frac{i}{2k_0}\left(\frac{1}{r_0} - \frac{1}{r}\right)k_\theta^2} U(r_0,k_\theta) \tag{4.33}$$

Coming back to space domain:

$$u(r,\theta) = e^{ik_0 \frac{\left(n^2-1\right)}{2}\Delta r} FT^{-1}\left\{ e^{-\frac{i}{2k_0}\left(\frac{1}{r_0} - \frac{1}{r}\right)k_\theta^2} FT\{u(r_0,\theta)\} \right\} \tag{4.34}$$

Where the turbulent phase screen is 1D and depends only on the azimuthal angle:

$$\phi(\theta,t) = k_0 \int_{r_0}^{r_0+\Delta r} n_1(\xi,\theta,t)\, d\xi \qquad \text{[rad]} \qquad (4.35)$$

Thus the general expression for *u* is (Fig.4.4):

$$u(r,\theta) = e^{i\phi(\theta,t)} FT^{-1}\left\{ e^{-\frac{i}{2k_0}\left(\frac{1}{r_0}-\frac{1}{r}\right)k_\theta^2} FT\{u(r_0,\theta)\} \right\} \qquad (4.36)$$

Comparing (4.36) to (4.16) one can note the same expression, considering that in 2D there is no dependence on φ.

This means that for the numerical scheme there is no explicit factor involved in the dimensional reduction, differently to what we found so far.

All the other observations concerning the propagation obviously are still valid. Similarly it is necessary to derive the spectrum of the phase variation. In such conditions:

$$B_{n_1}^{2D}(r,r\theta) = k_0^2 \int_{-\infty}^{+\infty} dk_r \int_{-\infty}^{+\infty} dk_\theta S_{n_1}^{2D}(k_r,k_\theta) e^{j(k_r r + k_\theta \theta)} = B_{n_1}^{3D}(r,r\theta,0) \qquad (4.37)$$

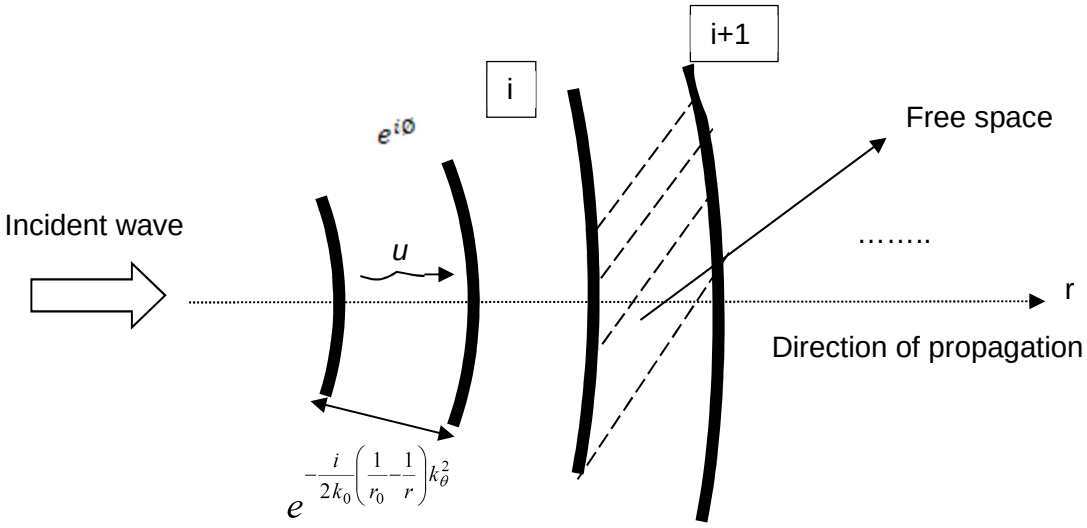

Figure 4. 3: *Scheme of the 2D model, 1D Multiple Phase Screens (2D PWE/ 1D MPS). Wave propagates in free space between two consecutive screens then its phase is modified by i-th screen*

and the dimensional reduction in the plane r-θ results in the vertical cross section of the 3D propagation medium. Ever since, following the approach developed above for 3D, it comes:

$$S_{\phi}^{1D}(k_{\theta}) = 2\pi k_0^2 \Delta r \frac{S_{n_1}^{2D}\left(k_r = 0, \frac{k_{\theta}}{r}\right)}{r} = \frac{2\pi k_0^2 \Delta r}{r} \int_{-\infty}^{+\infty} S_{n_1}^{3D}\left(k_r = 0, \frac{k_{\theta}}{r}, \frac{k_{\varphi}}{r}\right) dk_{\varphi} \tag{4.38}$$

Which can be compared to the result found in [19] for plane wave.

In particular, using Von Karman model (1.16):

$$S_{\phi}^{1D}(k_{\theta}) = \frac{2\pi k_0^2 \Delta r}{r} \times \frac{\sqrt{\pi}\Gamma(4/3)}{\Gamma(11/6)} 0.033 C_n^2 \left(\frac{k_{\theta}^2}{r^2} + K_{os}^2\right)^{-4/3} \approx \frac{2\pi k_0^2 \Delta r}{r} \times 0.055 C_n^2 \left(\frac{k_{\theta}^2}{r^2} + K_{os}^2\right)^{-4/3} \tag{4.39}$$

where Γ is the Gamma function.

The numerical scheme 2D-PWE/1D-MPS defined by (4.36) allows considering turbulence dependency with range through successive realisations of the 1D random phase screen $\phi(\theta)$ consistent with $S_{\phi}^{1D}(k_{\theta})$.

For the numerical theme, the spectrum is not 3D but a 2D version deriving from the compression of the overall energy of the turbulence in the vertical plane, as expressed in the integration on k_{φ} in equation (4.38).

All the processes treated in these two paragraphs are continuous obviously, but the simulator works in discrete domain. For this reason we expose some techniques to adapt the screen formulations made so far and some conditions for the numerical implementation.

4.3 Technical aspects for the numerical implementation

4.3.1 Reduced field realization

In compliance with the previous analysis of free-space propagation, phase screens are implemented from the beginning of the layer to the receiver: inside the layer both refractive and diffractive effects are present while from its end up to the receiver only the last one. Thus, for this last part of the link, we considered $\phi_i = 0$ in equations (4.16) and (4.36).

The idea is to propagate until the receiver the reduced field taken equal to 1 on every point of the first screen. In order to calculate numerically log-amplitude and phase variances we used the well-known relations considering the reduced field on the last screen:

$$\left\langle \chi^2 \right\rangle = Var\left\{20\log_{10}|u|\right\} \qquad [\text{dB}^2] \tag{4.40}$$

$$\left\langle \varphi^2 \right\rangle = Var\left\{ \arctan\left(\frac{\mathrm{Im}(u)}{\mathrm{Re}(u)} \right) \right\} \qquad [\mathrm{rad}^2] \qquad (4.41)$$

Actually our simulator works in discrete domain so wavenumbers are, for 3D:

$$k_{i_\theta} = i\Delta k_\theta = \frac{2\pi}{\theta_n} \qquad (4.42)$$

$$k_{h_\varphi} = h\Delta k_\varphi = \frac{2\pi}{\varphi_m} \qquad (4.43)$$

Hence Discrete Fourier Transform (DFT) and its inverse (IDFT) for 2D are (1D is only azimuthal angle dependent):

$$DFT\{u(r, n\Delta\theta, m\Delta\varphi)\} = U(r, i\Delta k_\theta, h\Delta k_\varphi) = \frac{1}{2\pi}\sum_{n=1}^{N}\left(\frac{1}{2\pi}\sum_{m=1}^{M} u(r, n\Delta\theta, m\Delta\varphi) e^{-j\frac{2\pi(m-1)(h-1)}{M}\Delta\theta} \right) e^{-j\frac{2\pi(n-1)(i-1)}{N}\Delta\varphi} \qquad (4.44)$$

$$IDFT\{U(r, i\Delta k_\theta, h\Delta k_\varphi)\} = u(r, n\Delta\theta, m\Delta\varphi) = \frac{1}{N}\sum_{i=1}^{N}\left(\frac{1}{M}\sum_{h=1}^{M} U(r, i\Delta k_\theta, h\Delta k_\varphi) e^{j\frac{2\pi(m-1)(h-1)}{M}\Delta k_\varphi} \right) e^{j\frac{2\pi(n-1)(i-1)}{N}\Delta k_\theta} \qquad (4.45)$$

Where $\Delta\theta$, $\Delta\varphi$ and $\Delta k_\theta, \Delta k_\varphi$ are sampling intervals in angular and wavenumber domain respectively and $1 \le i, n \le N$, $1 \le h, m \le M$. In order to enlighten the computation we use the FFT, assuming N and M power of 2. In the Appendix C the explanation of the coefficients used in (4.44) and (4.45) is given.

Let's find $\Delta k_\theta, \Delta k_\varphi$. Comparing Fourier kernels of (4.16) and (4.44):

$$e^{-ik_{i_\theta}\theta_n} = e^{-i\frac{2\pi(n-1)(i-1)}{N}} \qquad (4.46)$$

$$k_{i_\theta}(n-1)\Delta\theta = \frac{2\pi(n-1)(i-1)}{N} \qquad (4.47)$$

where $\theta_n = (n-1)\Delta\theta$. So:

$$k_{\max_\theta} = k_{N_\theta} = \frac{2\pi}{N\Delta\theta}(N-1) = \frac{2\pi}{\theta_{\max}}(N-1) \qquad (4.48)$$

$$\Delta k_\theta = \frac{k_{\max\,\theta}}{(N-1)} = \frac{2\pi}{\theta_{\max}} \tag{4.49}$$

Using the same approach for φ:

$$k_{\max\varphi} = \frac{2\pi}{M\Delta\varphi}(M-1) = \frac{2\pi}{\varphi_{\max}}(M-1) \tag{4.50}$$

$$\Delta k_\varphi = \frac{k_{\max\,\varphi}}{(M-1)} = \frac{2\pi}{\varphi_{\max}} \tag{4.51}$$

$\theta_{\max}$ and $\varphi_{\max}$ are the azimuthal and longitudinal aperture angles respectively, as illustrated in Fig.4.5.

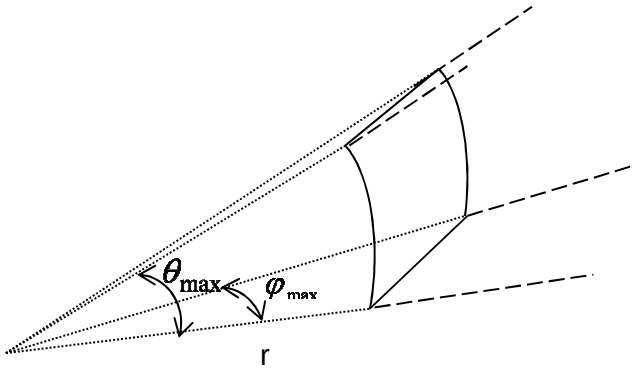

Figure 4. 4: Aperture angles for our geometry.

4.3.2 Criteria for phase screens

The application of the MPS propagation code requires that the field and the phase be specified at a discrete number of grid points. The number and spacing of these points must satisfy the following criteria, adapted from the ones of [26]:

1) Phase distribution of a screen must adequately represent the actual phase
2) Wave must propagate without angular aliasing
3) Edge effects or angular scattering off the end of the grid must be minimal.

1) Phase representation:

   a) Adequate phase representation is assured if each phase-screen length L is at least 5 to 10 times as large as the phase correlation distance or equivalently the outer scale:

$$L_i > 5L_{os} \quad \text{[m]} \tag{4.52}$$

where $L_i = r_i \theta_{\max}$ [m]is the dimension of the i-th screen. Due to the geometry of the scheme, illustrated in Fig.4.6, it is enough applying this condition at the first screen as the others increase the dimension with increasing distance.

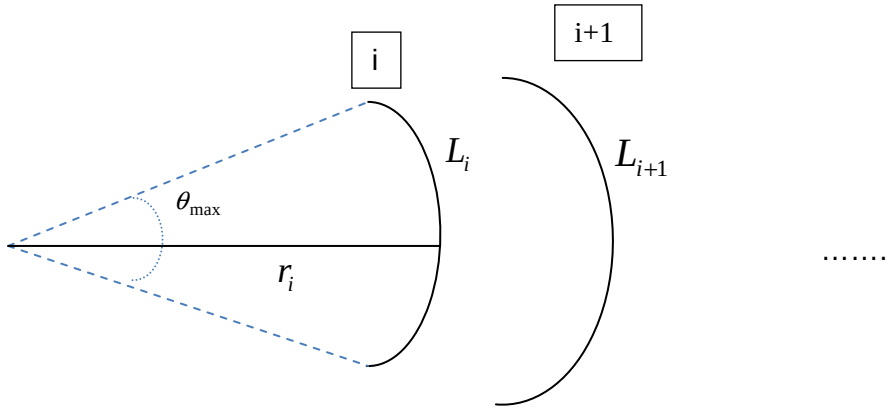

Figure 4. 5: Condition for the screens dimension

b) At a given distance r, the change in phase from one grid point at $\breve{y}_n = r\theta_n$ [m] to the next should be less than π to satisfy the Nyquist sampling theorem. Mathematically:

$$\phi(\breve{y}_2) - \phi(\breve{y}_1) < \pi \qquad \text{[rad]} \qquad (4.53)$$

where $\breve{y}_1 = r\theta_1$ and $\breve{y}_2 = r\theta_2$. In terms of the distance:

$$\Delta\breve{y} = \breve{y}_2 - \breve{y}_1 = r\Delta\theta \qquad \text{[m]} \qquad (4.54)$$

between two samples, this constraint can be written:

$$\Delta\breve{y}\left|\frac{\partial\phi}{\partial\breve{y}}\right| < \pi \qquad \text{[rad]} \qquad (4.55)$$

The variance of the derivative of the phase is related to the phase autocorrelation function [27]:

$$\left\langle\left(\frac{\partial\phi}{\partial\breve{y}}\right)^2\right\rangle = -\frac{d^2 B_\phi(\breve{y})}{d\breve{y}^2}\bigg|_{\breve{y}=0} \qquad \text{[rad}^2\text{/m}^2\text{]} \qquad (4.56)$$

Thus in a mean-square sense, the above limit on the grid spacing $\Delta\breve{y}$ may be expressed as:

$$\Delta\breve{y} < \pi\left(-\frac{d^2 B_\phi(\breve{y})}{d\breve{y}^2}\bigg|_{\breve{y}=0} \right)^{-\frac{1}{2}} \quad \text{[m]} \qquad (4.57)$$

In this case it is enough applying the condition for the biggest sample which is the one taken on the last screen, the biggest one, as shown in Fig.4.7.

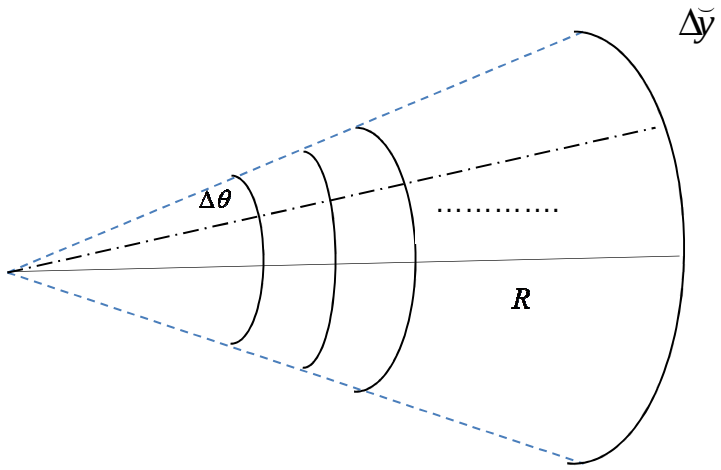

Figure 4. 6: Nyquist condition. Sample on the last screen is the main problem

2) Wave Propagation:

In order to adequately represent propagation in free space by the use of the Fourier transform relationships of (4.16) and (4.36), it is necessary that the various functions involved be accurately sampled. To satisfy the Nyquist sampling criterion, the difference in the function:

$$\frac{1}{2k_0}\left(\frac{1}{r_{i-1}} - \frac{1}{r_i}\right)\kappa^2 \qquad (4.58)$$

must be less than π when evaluated from one value of κ to the previous. Since the κ values are centred on zero, the maximum is in $\kappa_{\max} = \frac{N}{2}\kappa$ where N is the number of grid points. Hence the necessary condition is:

$$\frac{1}{2k_0}\left(\frac{1}{r_{i-1}} - \frac{1}{r_i}\right)\left(\frac{N}{2}\kappa\right)^2 - \frac{1}{2k_0}\left(\frac{1}{r_{i-1}} - \frac{1}{r_i}\right)\left(\frac{N-1}{2}\kappa\right)^2 < \pi \qquad (4.59)$$

which gives for 1D MPS:

$$\frac{1}{r_{i-1}} - \frac{1}{r_i} < \frac{4\theta_{\max}^2}{\lambda(N_\theta - 1)} \quad [m^{-1}] \quad (4.60)$$

and for 2D MPS:

$$\frac{1}{r_{i-1}} - \frac{1}{r_i} < \frac{4}{\lambda\left[\frac{(N_\theta - 1)}{\theta_{\max}^2} + \frac{(N_\varphi - 1)}{\varphi_{\max}^2}\right]} \quad [m^{-1}] \quad (4.61)$$

To find the restrictive condition we have to consider that:

$$r_{i-1} = r_i - \Delta r \quad [\text{m}] \quad (4.62)$$

So the difference between the reciprocal distances is:

$$\frac{1}{r_{i-1}} - \frac{1}{r_i} = \frac{\Delta r}{r_i(r_i - \Delta r)} \quad [m^{-1}] \quad (4.63)$$

Clearly, there is no need to apply the condition at each step but it is enough to do that on the highest value of (4.63, i.e. for the smallest distance r_i .

However this condition may be relaxed in practice if the phase spectrum is very small at large values of the wavenumber κ . In that case, the high wavenumber values are cut off by the phase power spectrum and small inaccuracies in the phase spectrum are relatively unimportant.

3) Edge Effects:

Because of the discrete nature of the MPS grid representation, energy leaving one side of the grid appears on the other side. As the propagation distance r increases, this effect becomes more important. This aliasing must be controlled for a propagation solution to be valid. Since the scattering angle is given by:

$$\nu = \frac{1}{k_0}\frac{\partial \phi}{\partial \breve{y}} \quad (4.64)$$

where ϕ is the phase at a general screen. The energy scattered at an angle ν travels a distance r ν perpendicular to the direction of propagation after propagating a distance r. To adequately

insure against edge effects it is necessary that the MPS grid size L be greater than rν for each propagation step. Thus:

$$L_i > \frac{r_i}{k_0}\left|\frac{\partial \phi}{\partial \breve{y}}\right| \quad \text{[m]} \qquad (4.65)$$

This expression may be represented in a mean-square sense using (4.17):

$$L_i > \frac{r_i}{k_0}\left(-\frac{d^2 B_\phi(\xi)}{d\xi^2}\bigg|_{\xi=0}\right)^{\frac{1}{2}} \quad \text{[m]} \qquad (4.66)$$

As for condition 1a), it is sufficient to consider the smallest screen, the first one which is placed at the shortest distance from the transmitter.

Often using of guard bands on the edges of the grid is a helpful tool but is not required to prevent aliasing.

4.3.3 Screens realization

The numerical technique to generate a 1D or 2D phase-screen realization of the MPS propagation code was developed at ONERA. The goal is to generate a stationary, random function $\phi(n\Delta\theta, m\Delta\varphi, t)$ which represents the phase evaluated along the MPS grid, sampled along longitudinal and azimuthal angles at steps $\Delta\theta$ and $\Delta\varphi$ with n and m representing the n-th and m-th point on the grid.

After generating a complex White Gaussian Noise (WGN) by the method described in [28] and assuming a discrete form $S_\phi^{2D}(\frac{k_{i_\theta}}{r_c}, \frac{k_{h_\varphi}}{r_c})$ of (4.26), the Fourier transform of the phase is defined as [29]:

$$\Phi\left(i\Delta k_\theta, h\Delta k_\varphi, t\right) = \sqrt{\frac{S_\phi^{2D}(\frac{k_{i_\theta}}{r_c}, \frac{k_{h_\varphi}}{r_c})}{\Delta k_\theta \Delta k_\varphi}}\, WGN \qquad (4.67)$$

Where r_c is the distance from the transmitter, increasing at each iteration c=1,2,..Ns; in other words $r_c = c\Delta r$.

Applying the Inverse Discrete Fourier Transform (4.45), we obtain:

$$\phi(n\Delta\theta, m\Delta\varphi, t) = IDFT\left\{\Phi(i\Delta k_\theta, h\Delta k_\varphi, t)\right\} = \frac{1}{NM}\sum_{h=1}^{M}\sum_{i=1}^{N}\Phi(i\Delta k_\theta, h\Delta k_\varphi, t)e^{j\frac{2\pi(n-1)(i-1)}{N}}e^{j\frac{2\pi(m-1)(h-1)}{M}}\Delta k_\varphi \Delta k_\theta \quad (4.68)$$

In this way $\phi(n\Delta\theta, m\Delta\varphi, t)$ is the sum of a sequence of Gaussian variables so its real and imaginary parts both have a Gaussian or normal probability distribution. Since the phase of an individual phase screen is a real quantity, one may choose either the real or imaginary part of $\phi(n\Delta\theta, m\Delta\varphi, t)$calculated in this manner saving computational time. It can be shown [30], [31] that the choice of $\Phi(i\Delta k_\theta, h\Delta k_\varphi, t)$, mentioned previously, gives the phase $\phi(n\Delta\theta, m\Delta\varphi, t)$as a stationary random process whose spectrum is $S_\phi^{2D}(\frac{k_{i_\theta}}{r_c}, \frac{k_{h_\varphi}}{r_c})$. Note that the spectrum of an individual phase-screen realization is not identically the desired PSD; however, the average of many realizations is indeed $S_\phi^{2D}(\frac{k_{i_\theta}}{r_c}, \frac{k_{h_\varphi}}{r_c})$. An alternative choice of $\phi(n\Delta\theta, m\Delta\varphi, t)$ involving replacement of the random quantity WGN, with a complex exponential of uniform phase would identically yield $S_\phi^{2D}(\frac{k_{i_\theta}}{r_c}, \frac{k_{h_\varphi}}{r_c})$ for the spectrum of every phase- screen realization [32]. In our simulator the IDFT is computed without considering the differentials $\Delta k_\varphi \Delta k_\theta$ so that, under this assumption and substituting (4.67) in (4.68) we create a 2D random phase screen:

$$\phi(n\Delta\theta, m\Delta\varphi, t) = IDFT_s\left\{\sqrt{S_\phi^{2D}(\frac{k_{i_\theta}}{r_c}, \frac{k_{h_\varphi}}{r_c})}WGN\sqrt{\Delta k_\theta}\sqrt{\Delta k_\varphi}\right\} \quad (4.69)$$

Where we called $IDFT_s$ the IDFT used by our simulator.

For 1D screen we use the same steps getting:

$$\phi(n\Delta\theta, t) = IDFT_s\left\{\sqrt{S_\phi^{2D}(\frac{k_{i_\theta}}{r_c})}WGN\sqrt{\Delta k_\theta}\right\} \quad (4.70)$$

Now we have all the elements to compute the numerical propagation of a spherical wave through a turbulent layer. In the following chapter we present the result of this method compared with the analytical expressions found in Chapter 2.

Chapter 5

Comparison between analytical and numerical methods

In the following section we compare the formulas derived analytically in Chapter 2 (2.36) -(2.38), (2.41)-(2.42) for 3D and (2.53)-(2.54), (2.55)-(2.56) for 2D with the results found by simulations using equations of Chapter 4 ((4.16) and (4.36)), only considering spherical wave either in Fraunhofer or Fresnel regime.

5.1 System characteristics

In this paragraph we present our results concerning a system working in 15km path with frequency varying from 5- to 30GHz, the Fresnel number from 0.1 to 10 and consequently the outer scale Los from 1 to 300m. The turbulent layer is 1km wide and it is located for three different positions:

a) 0.1km far from the transmitter

b) 7km far from the transmitter

c) 0.1km far from the receiver (13.9km from the transmitter)

It means we chose the main scenarios, i.e. when the irregularities are at the transmitter's and receiver's side and when they are in the middle of the path, in order to compare these results to the ones of Chapter 3[2]. Inner scale is fixed to 1mm and C_n^2 is constant and equal to $10^{-12} m^{-\frac{2}{3}}$ inside the layer.

A fundamental parameter is the aperture angle directly related to the dimension of the screens. For this reason we decided the height of the first screen and thanks to elevated distance transmitter-receiver (narrow angle) it was possible to use paraxial approximation getting the angular aperture. For the first screen dimension a value equal to $5\max\left(L_{os}, \sqrt{\lambda R}\right)$ was enough for our purpose.

We already discuss about the importance of the number of screens. In our case it was not the same along the path: 15 screens inside the layer and 8 from the layer to the receiver. The reason is that a lot

[2] In chapter 3 cases (a) and (c) considered the layer on the transmitter and on receiver respectively. Here it is not possible to use the same value for the first case because of numerical problem so we decide to enhance the distance in both cases to be coherent with the discussion.

of screens are useful to describe signal variations inside the turbulence, in compromise with computational time. On the contrary, in the last part of the communication there is no classical free-space propagation because of the diffraction due to Huygens' Principle already explained in par.3.2.1. The latter is not so strong hence few screens are enough. From transmitter to the turbulence no screen is present as here there is free-space propagation.

A numerical problem was based on dimensional configurations. For 3D we have 1024x1024 points per each 2D-screen so that we get smooth curves with few iterations per abscissa value; on the contrary for 2D we must use 1024 Monte-Carlo repetitions to get a better representation, as the 1D-screens have only 1024 points.

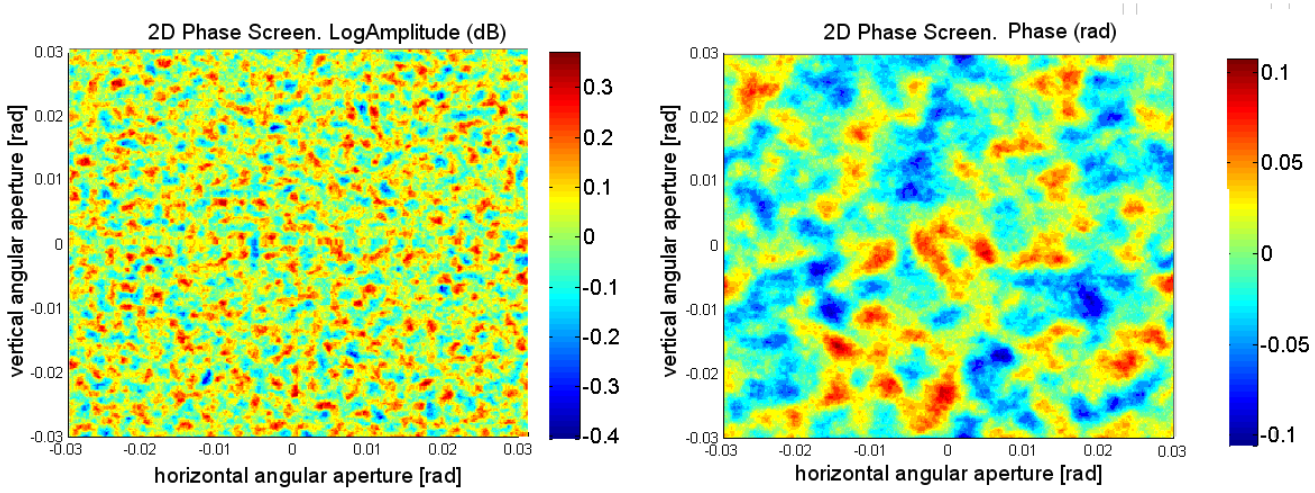

Figure 5. 1: 2D phase screen on the receiver. It is possible to note the variation of phase and log-amplitude due to the irregularities

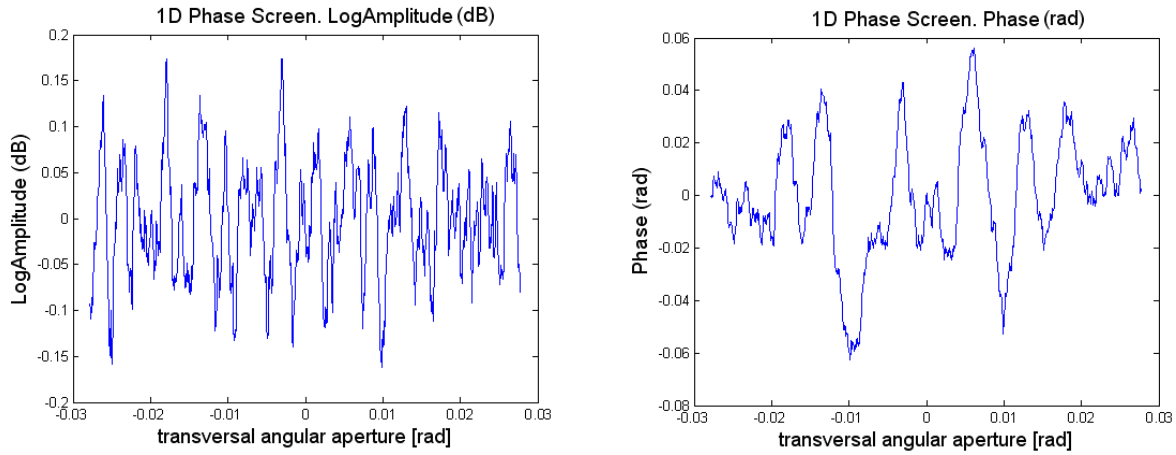

Figure 5. 2: Variation of log-amplitude and phase along the transverse direction on the last 1D screen

In Fig.5.1 and Fig.5.2 we show the variability of the process. They are one realization on the last 2D and 1D phase screens for case b) with a fixed frequency equal to 5GHz, Los 100m. It means Fresnel regime with Fresnel number equal to 0.3.

Fig.5.1 represents the 2D screen where the axes are the vertical and horizontal angular distances from the direct path. The variation of phase and amplitude can be noticed for the different colours in a range -0.4/+0.3 and +/-0.1 respectively. The independence of the two processes is clear because of the different weighting functions involved: for phase even small wavenumbers are important differently from log-amplitude.

Another characteristic is that the variations are not sparse due to modelling of the turbulence in random correlated Gaussian noise; zones coloured by red denote dense irregularities.

On the other hand, in Fig.5.1 variations are defined on the ordinates depending on the transverse direction. By this plot, the fast fluctuation of the log-amplitude around the average value are more evident.

5.2 Graphical representations

In the figures below three kinds of curves are shown for log-amplitude and phase variances for 3D and 2D:

- numerical green), concerning the simulation of the propagation of the reduce field *u*

- asymptotic Fresnel (black) and Fraunhofer (red), from equations (2.36)-(2.38), (2.41)-(2.42) for 3D and (2.53)-(2.54), (2.55)-(2.56) for 2D

- full analytical (blue)

The last one is considered because log-amplitude and phase variances computed in Chapter 2 are only asymptotic formulas: for Fresnel regime, spectrum was based on Kolmogorov model not the complete Von Karman's while in Fraunhofer regime the weighting functions were approximated to the value 0.5. For such a reason, with the help of the simulator, we can plot also the complete analytical curves from equations (2.21)-(2.22) for 3D and (2.49)-(2.50) for 2D**.**

This time we want to study the fluctuation of the variances depending on the frequency and outer scale so the abscissa stands for the Fresnel number $\frac{\sqrt{\lambda R}}{L_{os}}$. As expressed in the previous chapters when it is lower than 1 we are in Fresnel regime, otherwise we are in Fraunhofer's. Log-amplitude variances are

normalized by $C_n^2 k_0^2 K_{os}^{\frac{-5}{3}}$ and phase variances by C_n^2 in order to have a clearer representation. x1, x2 are the distances from the transmitter to the beginning and to the end of the turbulent layer.

- **Log-amplitude :**

a) Transmitter side: R=15km x1=1km x2=2km

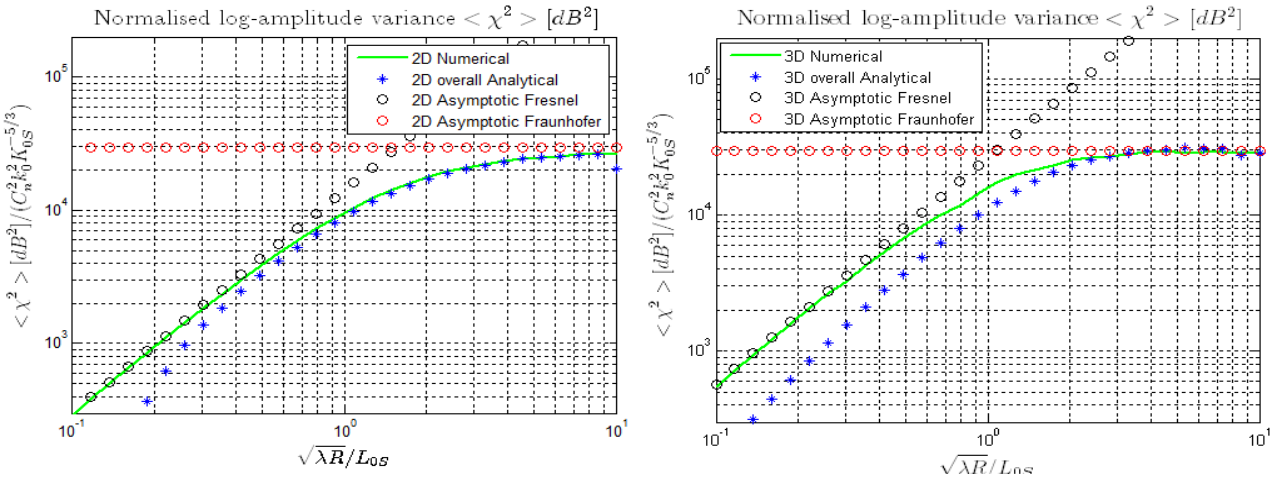

Figure 5. 3: Log-amplitude variances when the layer is near the transmitter

b) Mid-distance: R=15km x1=7km x2=8km

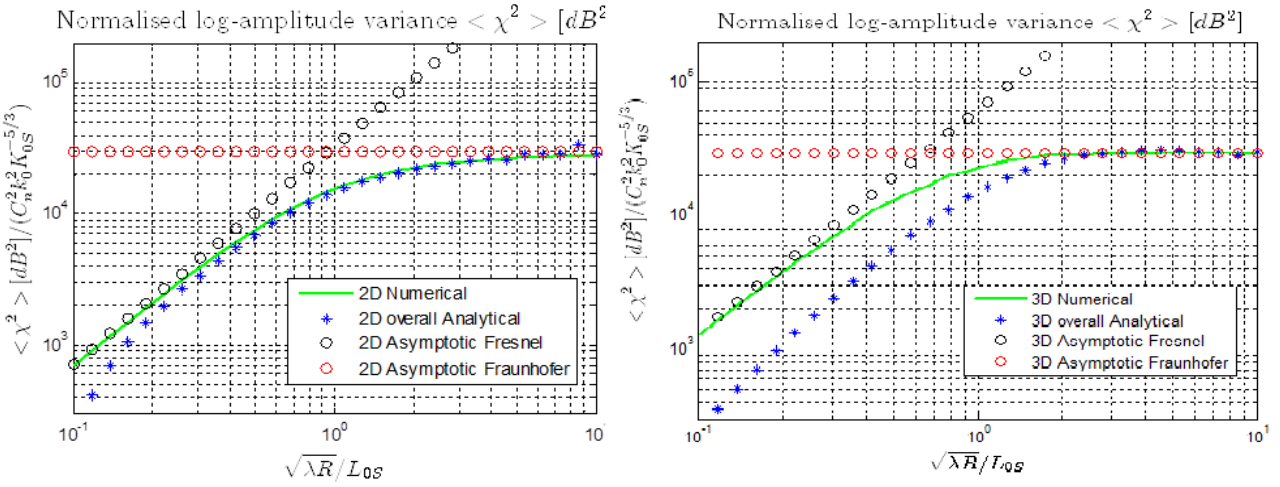

Figure 5. 4: Log-amplitude variances when the layer is in the middle of the link

c) Receiver side: R=15km x1=13km x2=14km

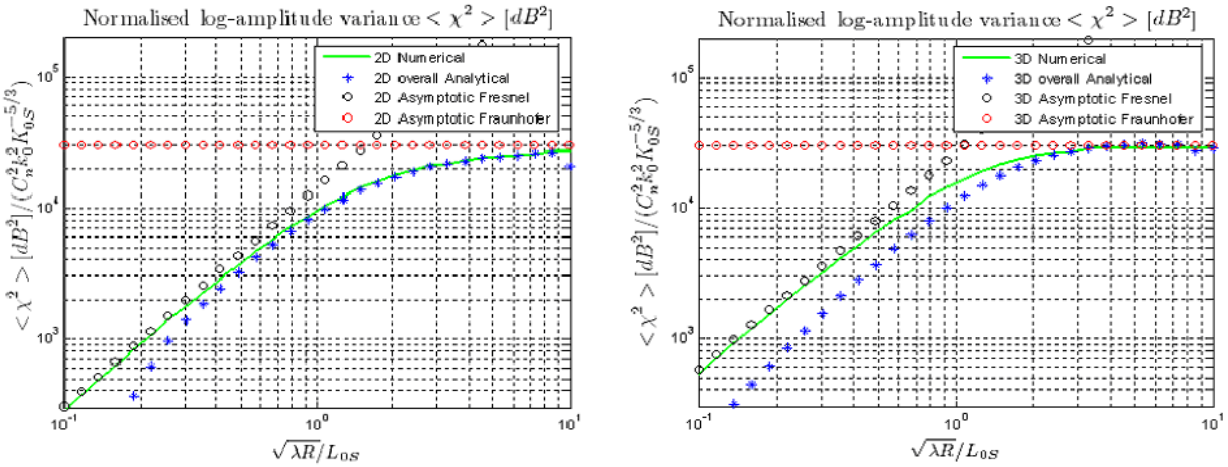

Figure 5. 5: Log-amplitude variances when the layer is near the receiver.

The numerical curves do not match perfectly with the full analytical ones; this is probably due to the fact that a finite interval has been considered to calculate numerically the integral in the expressions (2.21) and (2.49). In 3D the mismatch is more severe. Anyway, comparing the numerica curves with the asymptotical ones we find a validation of our model.
Observing the course of the function, it is clear the effect of the normalization:

- in Fraunhofer side, variance is constant and depends only on the thickness of the layer, so that the convergence value is always the same in all figures.

- -in Fresnel side, variance increases exponentially (linearly in log-scale), in fact it is function of the variables K_{os} and ko:

$$\left\langle \chi^2 \right\rangle_{fresnel} \sim \frac{k_0^{\frac{7}{6}}}{k_0^2 K_{os}^{-\frac{5}{3}}} = k_0^{-\frac{5}{6}} K_{os}^{\frac{5}{3}} = \left(\sqrt{2\pi} \frac{\sqrt{\lambda}}{L_{os}} \right)^{\frac{5}{3}} \qquad [\text{Np}^2] \qquad (5.1)$$

which is an increasing function, considering an increasing abscissa $\frac{\sqrt{\lambda R}}{L_{os}}$ with decreasing λ and L_{os}. In this regime there are validations of two points of our discussion: the error due to the dimensional reduction from 3D to 2D and the reciprocity of the log-amplitude variance for spherical wave. For the first point it is clear that 2D curves are lower than the 3D ones because of the factor already mentioned. About the reciprocity it can be noticed that case a) and case c)

lead to the same variances and in these typesetting they are also the minimal, while in case b) when the layer is at mid-path, the variance is higher. This result complies with the observation exposed in Chapter II.

- **Phase**

a) Transmitter side: R=15km x1=1km x2=2km

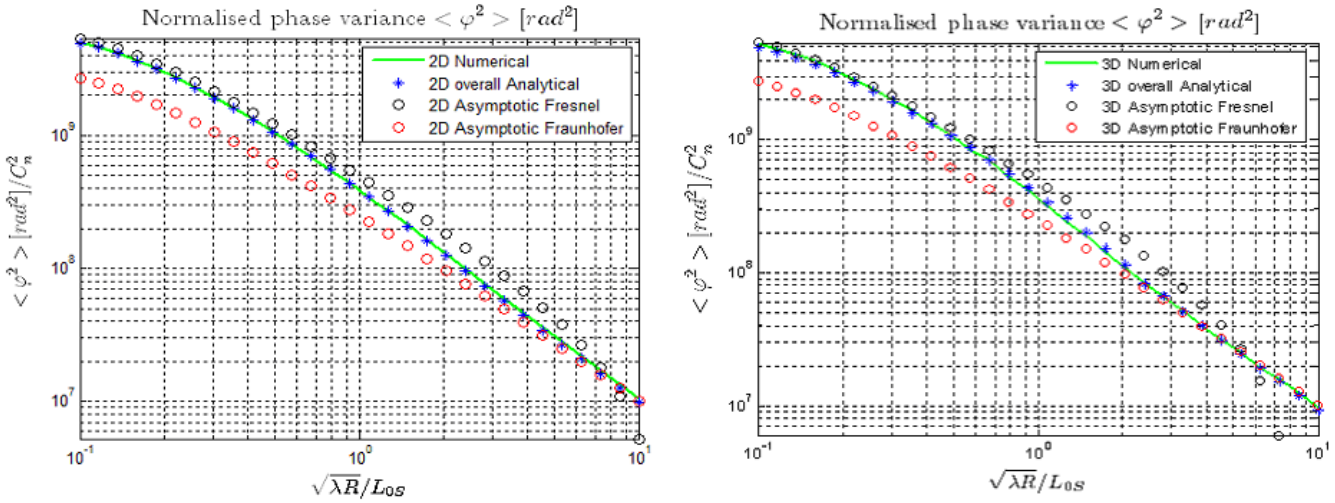

Figure 5. 6: Phase variances when the layer is near the transmitter

b) Mid-distance: R=15km x1=7km x2=8km

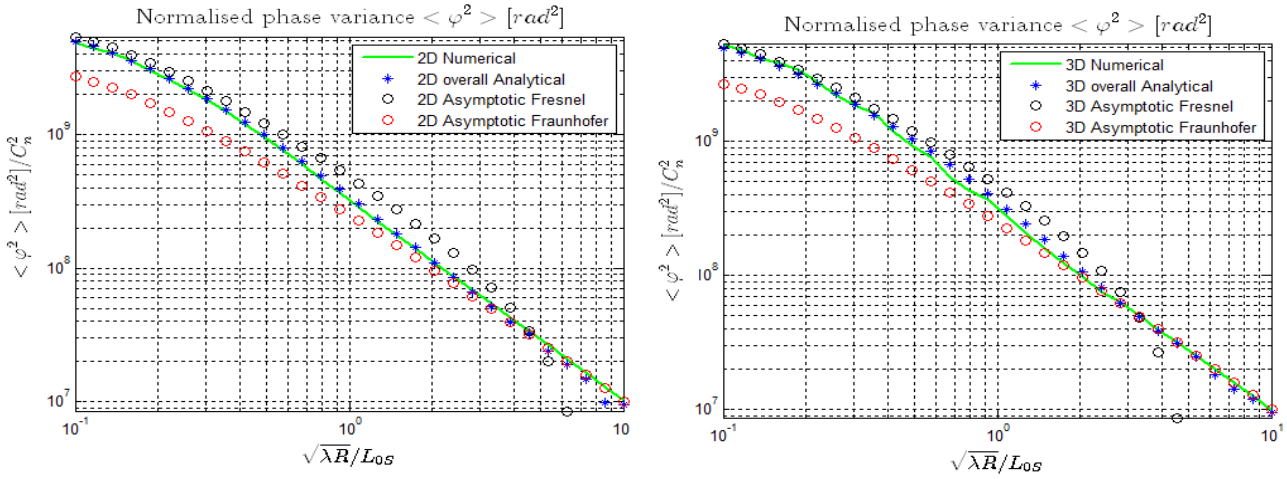

Figure 5. 7: Phase variances when the layer is in the middle of the link.

c) Receiver side: R=15km x1=13km x2=14km

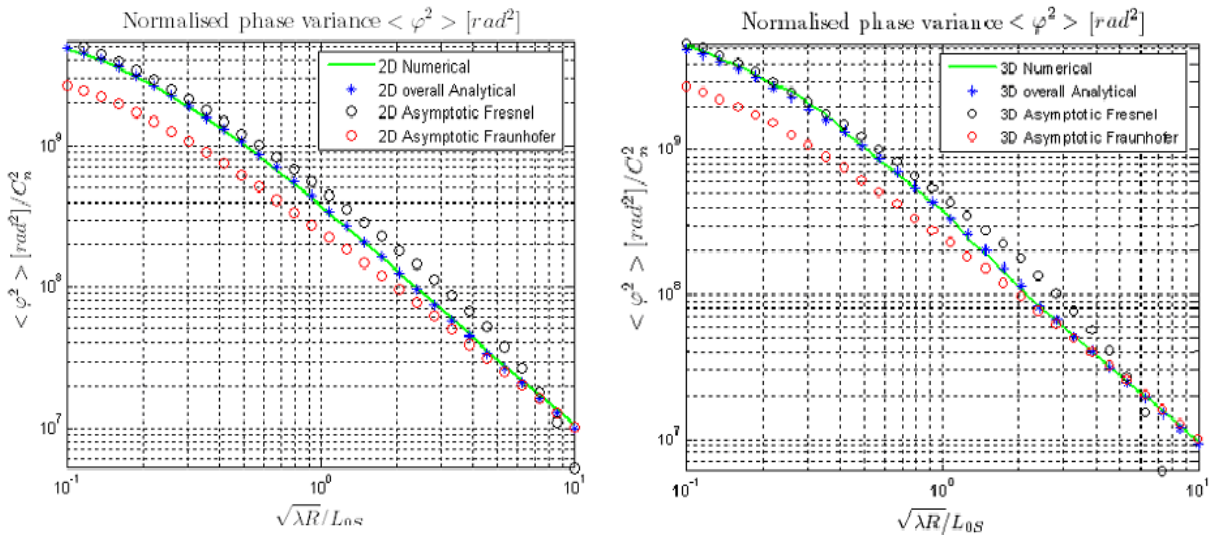

Figure 5. 8: Phase variances when the layer is near the receiver

This time the normalization term is the constant C_n^2 so that the effect is only a translation of the plot.

- in Fresnel regime variance decreases as:

$$\left\langle \varphi^2 \right\rangle_{fresnel} \sim k_0^2 K_{os}^{-\frac{5}{3}} - k_0^2 k_0^{-\frac{5}{6}} = k_0^2 K_{os}^{-\frac{5}{3}} - k_0^{\frac{7}{6}} \qquad [\text{rad}^2] \qquad (5.2)$$

- in Fraunhofer regime variance is still decreasing because of the dependence on:

$$k_0^2 K_{os}^{-\frac{5}{3}} \qquad (5.3)$$

Hence phase variance generally decreases with increasing Fresnel number, becoming really low when Fraunhofer regime is clearly defined.

Here the numerical curve matches the analytical in both configurations.

It is not possible to see the reciprocity of the spherical wave because for all the three cases variance is the same both for 2D and 3D, in compliance with observations in par.2.2.1.2.

The difference between 2D and 3D is barely noticeable so in Fig.5.9 we superposed the two numerical variances for case c) as an example. The error is negligible so for the phase there is no problem introducing a dimensional reduction both in Fresnel and Fraunhofer regime.

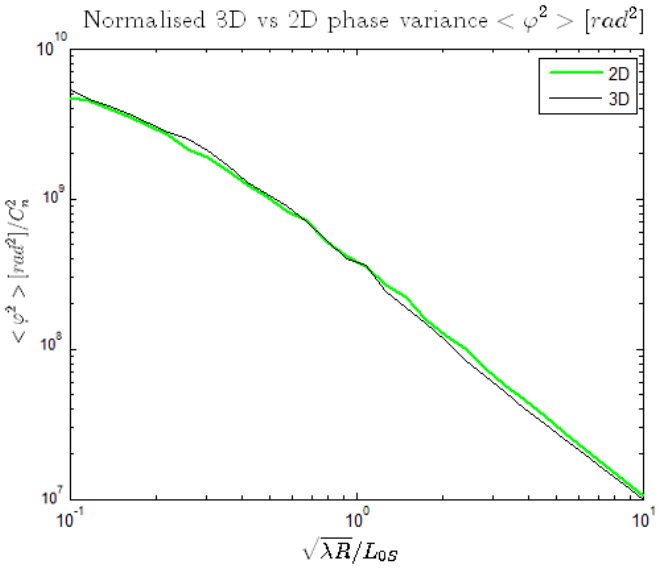

Figure 5. 9: Phase variances for 2D and 3D in case c). They almost match, so 2D is a good approximation of real 3D

Conclusion

The aim of the work was to study the scintillation for an incident spherical wave on a general tropospheric turbulence placed in a limited part of the communication. This is useful for terrestrial links or satellite uplinks where the irregularities are near the emitter and it is not possible to consider the plane wave approach. On the contrary, great efforts were already made to study scenarios where turbulence is near the receiver, as for satellite downlink or optical astronomy, always considering plane wave due to the distances involved.

Firstly log-amplitude and phase variances have been derived analytically under weak scattering assumption, examining in detail how they change in relation to different parameters (wavelength, path length, etc..) and different configuration (3D or 2D). Then we compared our results to the ones already developed for plane wave finding points in common and differences.

After that, we develop a numerical model based on the Parabolic Wave Equation combined with Multiple Phase Screens that allows studying scintillation effects whatever the regime.

Finally we compare the results of the two methods by simulations in order to validate the model.

As commonly known, when the distance of the link is high, plane wave can be considered to detect the field at the receiver. Nevertheless we found out that the main problem does not concern the overall distance but the position of the layer along the path: only when it is not so much extended and when it is near the receiver the approximation is valid, obviously getting better for high distance transmitter-receiver. In this case variances are the same, thus simplified model of plane wave is a useful tool. For this reason the real case of the spherical wave is overestimated for log-amplitude and underestimated for phase for all the other positions of the layer. In slab configuration the difference was quantitatively calculated as equal to 40%, but in our condition it is not constant, in fact it decreases with increasing distance transmitter-turbulences, starting with the worse value when perturbation is near the source.

One important property of the spherical wave is the reciprocity, not present in the plane wave. This means that assuming two different scenarios where the turbulence is near the transmitter and where it is near the receiver, the log-amplitude and phase variances will be same. Actually we noticed that reciprocity influences most the log-amplitude than the phase due to the connection between the corresponding weighting functions and the spectrum of the fluctuations of refractive index. In fact it has high energy for small wavenumbers which are more important for phase weighting function, then it decreases rapidly to really small values. Hence, phase variance is considered constant whatever the position of the irregularities, log-amplitude variance symmetrical with respect the middle path where it is maxima. This point is valid only for Fresnel regime because we saw that in Fraunhofer zone variances are always the same for any position of the irregularities, in fact they only depend on the thickness of the turbulent layer.

The other theme was the analysis of the use of 2D instead of 3D configuration. We found the same results of the plane wave: in Fresnel regime for log-amplitude variance the factor 1.86 and for phase variance a negligible error, in Fraunhofer regime no changes. It implies that dimensional reduction has the same effect independently of the wave considered.

In conclusion, scintillation has the same effect on phase in both regimes regardless of the spatial configuration and the position of the turbulent layer. On the other hand, amplitude variation keeps the same behaviour only in Fraunhofer but not in Fresnel regime, where it changes according to these characteristics.

In Fraunhofer regime plane wave is always a good approximation but in Fresnel regime its use is restricted only when the irregularities are near the receiver and if the turbulence does not cover a big part of the link.

Some points can implemented in the future. First of all, we have considered a constant value for C_n^2 in the spectrum formulation, but actually it varies in dependence on the altitude. So it is possible to divide a layer with different values of C_n^2 into sublayers with the a constant value and applying our model for each of them.

Anisotropy of the spectrum can be introduced, as we have considered isotropy assumption.

Lastly other elements in geometry can be treated, as the multipath deriving from the reflections of the ground or the antenna pattern etc.

Appendix A

Here we show the calculations which lead to the expression of log-amplitude and phase variances in 3D scenario for a spherical incident wave.

From equations (2.15)-(2.18) amplitude and phase are:

$$\chi(\vec{R},t) = -2k_o^2 \int d^3r.n_1(\vec{r},t).A(\vec{R},\vec{r}) \qquad \text{[Np]} \qquad \text{(A.1)}$$

$$\varphi(\vec{R},t) = -2k_o^2 \int d^3r.n_1(\vec{r},t).B(\vec{R},\vec{r}) \qquad \text{[rad]} \qquad \text{(A.2)}$$

where

$$A(\vec{R},\vec{r}) = \Re\left[G^{3D}(\vec{R},\vec{r}) \frac{E_o(\vec{r})}{E_o(\vec{R})} \right] \qquad [m^{-1}] \qquad \text{(A.3)}$$

and

$$B(\vec{R},\vec{r}) = \Im\left[G^{3D}(\vec{R},\vec{r}) \frac{E_o(\vec{r})}{E_o(\vec{R})} \right]. \qquad [m^{-1}] \qquad \text{(A.4)}$$

with $G^{3D}(\vec{R},\vec{r}), E_0(\vec{r}), E_0(\vec{r})$ are defined in (2.16), (2.19), (2.20).

Therefore, 3D log-amplitude variance $<\chi^2(\vec{R},t)>^{3D}$ is given by:

$$\begin{aligned} <\chi^2(\vec{R},t)>^{3D} &= 4k_o^4 \int d^3r.A(\vec{R},\vec{r}) \int d^3r'.A(\vec{R},\vec{r}') < n_1(\vec{r},t) n_1(\vec{r}',t) > \\ &= 4\int d^3k.S_{n_1}^{3D}(\vec{k}) D^{3D}(\vec{k}) D^{3D}(-\vec{k}) \end{aligned} \qquad \text{[Np]} \qquad \text{(A.5)}$$

Where $S_{n_1}^{3D}(\kappa)$ is the spectrum of n_1, defined in (2.16) and:

$$D^{3D}(\vec{k}) = k_o^2 \int d^3r.A(\vec{R},\vec{r}) e^{i\vec{k}.\vec{r}}. \qquad \text{(A.6)}$$

Similarly, phase variance $<\varphi^2(\vec{R},t)>^{3D}$:

$$<\varphi^2(\vec{R},t)>^{3D} = 4\int d^3k.S_{n_1}^{3D}(\vec{k}) E^{3D}(\vec{k}) E^{3D}(-\vec{k}), \qquad \text{[rad}^2\text{]} \qquad \text{(A.7)}$$

Where

$$E^{3D}(\vec{k}) = k_o^2 \int d^3 r.B(\vec{R},\vec{r}) e^{i\vec{k}.\vec{r}}. \tag{A.8}$$

To evaluate the products $D^{3D}(\vec{k})D^{3D}(-\vec{k})$ and $E^{3D}(\vec{k})E^{3D}(-\vec{k})$, we introduce $\Lambda^{3D}(\vec{k})$,defined as:

$$\Lambda^{3D}(\vec{k}) = D^{3D}(\vec{k}) + iE^{3D}(\vec{k}) = k_o^2 \int d^3 r G^{3D}(\vec{R},\vec{r}) \frac{E_o(\vec{r})}{E_o(\vec{R})} e^{i\vec{k}.\vec{r}}. \tag{A.9}$$

In such conditions:

$$2D^{3D}(\vec{k}) = \Lambda^{3D}(\vec{k}) + \Lambda^{3D*}(-\vec{k}) \tag{A.10}$$

and

$$2iE^{3D}(\vec{k}) = \Lambda^{3D}(\vec{k}) - \Lambda^{3D*}(-\vec{k}) \tag{A.11}$$

where * stands for complex conjugate.

Considering $\vec{k} \equiv (k_x, k_y, k_z)$, the x axis as the direct path transmitter/receiver ($\vec{R} \equiv (R,0,0)$) and assuming narrow scattering angles, R-x is greater than transverse dimensions y and z so that (2.16) and (2.19) reduce to:

$$G^{3D}(\vec{R},\vec{r}) = \frac{e^{ik_o|\vec{R}-\vec{r}|}}{4\pi|\vec{R}-\vec{r}|} \approx \frac{e^{ik_o(R-x)} e^{ik_o \frac{y^2+z^2}{2(R-x)}}}{4\pi(R-x)}. \qquad [m^{-1}] \tag{A.12}$$

$$E_0(\vec{r}) = \frac{E_0 e^{i\vec{k}\cdot\vec{r}}}{\vec{r}} = \frac{E_0 e^{ik_0\sqrt{x^2+y^2+z^2}}}{\sqrt{x^2+y^2+z^2}} = \frac{E_0 e^{ik_0 x} e^{ik_0 \frac{y^2+z^2}{2x}}}{x} \tag{A.13}$$

Consequently (A.9) becomes:

$$\Lambda^{3D}(\vec{k}) = \frac{k_0^2}{4\pi} \int_{x_1}^{x_2} \frac{e^{ik_x x} R}{x(R-x)} dx \int_{-\infty}^{\infty} e^{ik_y y} e^{\frac{ik_0 y^2 R}{2x(R-x)}} dy \int_{-\infty}^{\infty} e^{\frac{ik_0 z^2 R}{2x(R-x)}} e^{ik_z z} dz \tag{A.14}$$

Where the turbulence is limited in the region [x_1 , x_2] as shown in Fig.2.3.

Using the relationship:

$$\int_{-\infty}^{+\infty} du.e^{iau}.e^{ibu^2} = \sqrt{\frac{\pi}{b}}i \times e^{-i\frac{a^2}{4b}} \tag{A.15}$$

(A.14) reduces to:

$$\Lambda^{3D}\left(\vec{k}\right) = 0.5ik_0 \int_{x_1}^{x_2} e^{ik_x x} e^{i\frac{\left(k_y^2+k_z^2\right)}{2Rk_0}x(R-x)} dx \tag{A.16}$$

Defining the square of the wavenumber transverse to the direction of propagation $k_r^2 = k_y^2 + k_z^2$ and after a change of variables, it is possible to solve (A.10) and (A.11) as:

$$D^{3D}(\vec{k}) = [\Lambda^{3D}(\vec{k}) + \Lambda^{3D^*}(-\vec{k})]/2 = 0.5k_o e^{ik_x R} \int_{x_1}^{x_2} dx e^{-ik_x x} \sin\left(\frac{x(R-x)k_r^2}{2Rk_o}\right), \tag{A.17}$$

$$E^{3D}(\vec{k}) = [\Lambda^{3D}(\vec{k}) - \Lambda^{3D^*}(-\vec{k})]/2i = 0.5k_o e^{ik_x R} \int_{x_1}^{x_2} dx e^{-ik_x x} \cos\left(\frac{x(R-x)k_r^2}{2Rk_o}\right). \tag{A.18}$$

For (A.5) and (A.7), the two products have to be evaluated:

$$D^{3D}(\vec{k})D^{3D}(-\vec{k}) = \frac{k_o^2}{4}\int_{x_1}^{x_2} dx' \int_{x_1}^{x_2} dx'' e^{i(x''-x')k_x} \sin\left(\frac{x'\left(R-x'\right)k_r^2}{2Rk_o}\right)\sin\left(\frac{x''\left(R-x''\right)k_r^2}{2Rk_o}\right), \tag{A.19}$$

$$E^{3D}(\vec{k})E^{3D}(-\vec{k}) = \frac{k_o^2}{4}\int_{x_1}^{x_2} dx' \int_{x_1}^{x_2} dx'' e^{i(x''-x')k_x} \cos\left(\frac{x'\left(R-x'\right)k_r^2}{2Rk_o}\right)\cos\left(\frac{x''\left(R-x''\right)k_r^2}{2Rk_o}\right). \tag{A.20}$$

We introduce the sum and difference coordinates *u=x'' – x'* and *2x=x'' + x'*, and recalling trigonometric formulas:

$$\begin{aligned} D^{3D}(\vec{k})D^{3D}(-\vec{k}) &= \frac{k_o^2}{4}\int_{x_1}^{x_2} dx \int_{-f(x)}^{+f(x)} du e^{iuk_x}\left[\sin^2\left(\frac{x(R-x)k_r^2}{2Rk_o}\right) - \sin^2\left(\frac{x(R-x)k_r^2}{2Rk_o}\right)\right], \\ &= \frac{k_o^2}{4}\int_{x_1}^{x_2} dx \int_{-f(x)}^{+f(x)} du e^{iuk_x} \sin^2\left(\frac{x(R-x)k_r^2}{2Rk_o}\right) - \varepsilon \end{aligned} \tag{A.21}$$

$$\begin{aligned} E^{3D}(\vec{k})E^{3D}(-\vec{k}) &= \frac{k_o^2}{4}\int_{x_1}^{x_2} dx \int_{-f(x)}^{+f(x)} du e^{iuk_x}\left[\cos^2\left(\frac{x(R-x)k_r^2}{2Rk_o}\right) - \sin^2\left(\frac{x(R-x)k_r^2}{2Rk_o}\right)\right]. \\ &= \frac{k_o^2}{4}\int_{x_1}^{x_2} dx \int_{-f(x)}^{+f(x)} du e^{iuk_x} \cos^2\left(\frac{x(R-x)k_r^2}{2Rk_o}\right) - \varepsilon \end{aligned} \tag{A.22}$$

At optical and microwave frequencies, the double integral ε is negligible, so that:

$$D^{3D}(\vec{k})D^{3D}(-\vec{k}) = \frac{k_o^2}{2}\int_{x_1}^{x_2} dx \sin^2\left(\frac{x(R-x)k_r^2}{2Rk_o}\right)\frac{\sin[f(x)k_x]}{k_x} \quad \text{(A.23)}$$

$$E^{3D}(\vec{k})E^{3D}(-\vec{k}) = \frac{k_o^2}{2}\int_{x_1}^{x_2} dx \cos^2\left(\frac{x(R-x)k_r^2}{2Rk_o}\right)\frac{\sin[f(x)k_x]}{k_x} \quad \text{(A.24)}$$

Reminding of:

$$\delta(x - x_o) = \frac{1}{\pi}\lim_{\varepsilon \to 0}\left(\frac{\sin[(x - x_o)\varepsilon^{-1}]}{(x - x_o)}\right) \quad \text{(A.25)}$$

and due to $f(x).k_x >> 1$, we obtain:

$$2\left[\frac{\sin f(x)k_x}{k_x}\right] = 2\pi\delta(k_x) \quad \text{(A.26)}$$

$$D^{3D}(\vec{k})D^{3D}(-\vec{k}) = \frac{k_o^2}{4}\int_{x_1}^{x_2} dx \sin^2\left(\frac{x(R-x)k_r^2}{2Rk_o}\right)2\pi\delta(k_x) = \frac{\pi k_o^2}{2}\delta(k_x)\int_{x_1}^{x_2} dx \sin^2\left(\frac{x(R-x)k_r^2}{2Rk_o}\right) \quad \text{(A.27)}$$

$$E^{3D}(\vec{k})E^{3D}(-\vec{k}) = \frac{k_o^2}{4}\int_{x_1}^{x_2} dx \cos^2\left(\frac{x(R-x)k_r^2}{2Rk_o}\right)2\pi\delta(k_x) = \frac{\pi k_o^2}{2}\delta(k_x)\int_{x_1}^{x_2} dx \cos^2\left(\frac{x(R-x)k_r^2}{2Rk_o}\right)$$

(A.28)

So now we can solve the variance expressions:

$$<\chi^2>^{3D} = 4\int d^3k.S_n^{3D}(\vec{k})D^{3D}(\vec{k})D^{3D}(-\vec{k}) = 4\int d^3k.S_n^{3D}(\vec{k})\frac{\pi k_o^2}{2}\delta(k_x)\int_{x_1}^{x_2} dx \sin^2\left(\frac{x(R-x)k_r^2}{2Rk_o}\right) \quad [\text{Np}^2] \text{ (A.29)}$$

$$<\varphi^2>^{3D} = 4\int d^3k.S_n^{3D}(\vec{k})E^{3D}(\vec{k})E^{3D}(-\vec{k}) = 4\int d^3k.S_n^{3D}(\vec{k})\frac{\pi k_o^2}{2}\delta(k_x)\int_{x_1}^{x_2} dx \cos^2\left(\frac{x(R-x)k_r^2}{2Rk_o}\right) \quad [\text{rad}^2] \text{ (A.30)}$$

Passing to spherical coordinates (κ, ν, ω) where $k_r = \sqrt{k_y^2 + k_z^2} = \kappa\sin\nu$ and $k_x = \kappa\cos\nu$, as shown in Fig.A.1:

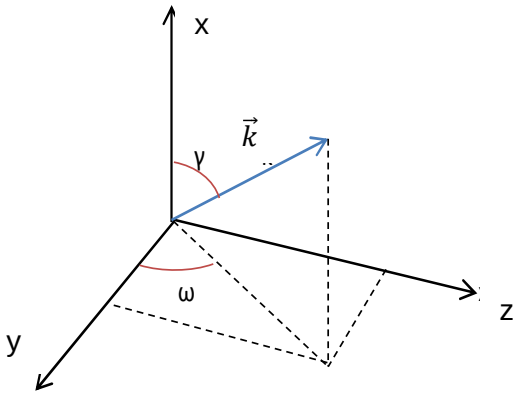

Figure A. 1: Spherical coordinate system with respect the wave-number $\vec{k}$

New formulations are:

$$< \chi^2 >^{3D} = 2\pi k_o^2 \int_0^{\infty} d\kappa S_{n_1}^{3D}(\kappa)\kappa^2 \int_0^{\pi} d\nu \sin\nu \int_0^{2\pi} d\omega \int_{x_1}^{x_2} dx \sin^2\left(\frac{x(R-x)\kappa^2 \sin^2\nu}{2Rk_o}\right)\delta(\kappa\cos\nu) \quad [\text{Np}^2] \quad (A.31)$$

$$< \varphi^2 >^{3D} = 2\pi k_o^2 \int_0^{\infty} d\kappa S_{n_1}^{3D}(\kappa)\kappa^2 \int_0^{\pi} d\nu \sin\nu \int_0^{2\pi} d\omega \int_{x_1}^{x_2} dx \cos^2\left(\frac{x(R-x)\kappa^2 \sin^2\nu}{2Rk_o}\right)\delta(\kappa\cos\nu) \quad [\text{rad}^2] \quad (A.32)$$

Because of the assumption of isotropy it can be considered $|\vec{k}|$ instead $\vec{k}$ so that $S_n^{3D}(\vec{k}) = S_n^{3D}(|\vec{k}|) = S_n^{3D}(\kappa)$.

Considering impulse properties, we get log-amplitude and phase variances (2.10):

$$< \chi^2 >^{3D} = 4\pi^2 k_o^2 \int_0^{\infty} d\kappa S_{n_1}^{3D}(\kappa)\kappa^2 \int_{x_1}^{x_2} dx \sin\nu_0 \frac{1}{\kappa\sin\nu_0} \sin^2\left(\frac{x(R-x)\kappa^2 \sin^2\nu_0}{2Rk_o}\right) = 4\pi^2 k_o^2 \int_0^{\infty} d\kappa S_{n_1}^{3D}(\kappa)\kappa \int_{x_1}^{x_2} dx \sin^2\left(\frac{x(R-x)\kappa^2}{2Rk_o}\right) \quad (A.33)$$

$$< \varphi^2 >^{3D} = 4\pi^2 k_o^2 \int_0^{\infty} d\kappa S_{n_1}^{3D}(\kappa)\kappa^2 \int_{x_1}^{x_2} dx \sin\nu_0 \frac{1}{\kappa\sin\nu_0} \cos^2\left(\frac{x(R-x)\kappa^2 \sin^2\nu_0}{2Rk_o}\right) = 4\pi^2 k_o^2 \int_0^{\infty} d\kappa S_{n_1}^{3D}(\kappa)\kappa \int_{x_1}^{x_2} dx \cos^2\left(\frac{x(R-x)\kappa^2}{2Rk_o}\right) \quad (A.34)$$

where $\nu_0 = \frac{\pi}{2}$ which means the interest is based on the transverse plane because the component along the direction of propagation $k_x = 0$ so $k_r = \kappa$, as shown in Fig, A.2. This can lead to a misunderstanding since during the discussion κ is presented implicitly as the transverse wavenumber not the complete one of Fig.A.1.

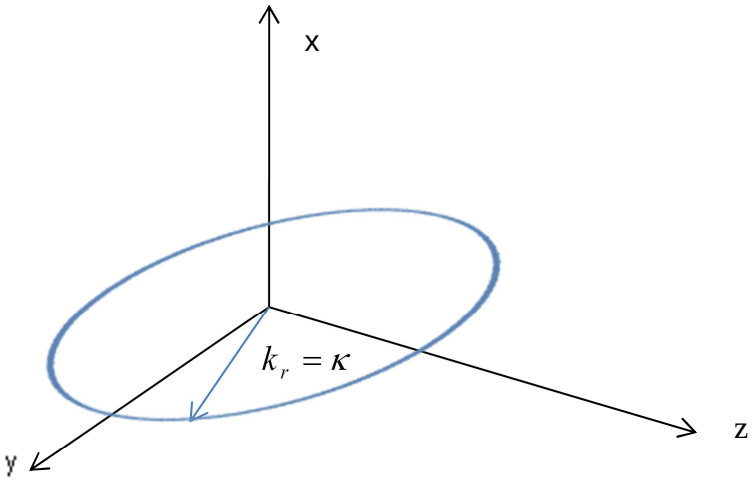

Figure A. 2: As $\nu_0 = \frac{\pi}{2}$, $\vec{k}$ *lies on the transversal plane y-z, so* $\kappa = k_r$

Appendix B

Here we want solve the integrals in x variable of (2.25) and (2.26), which lead to the expressions of the spherical weighting functions for phase and log-amplitude.

They are:

$$A = \int_{x_1}^{x_2} \sin^2\left(\frac{\kappa^2 x(R-x)}{2k}\right) dx \tag{B.1}$$

$$B = \int_{x_1}^{x_2} \cos^2\left(\frac{\kappa^2 x(R-x)}{2k}\right) dx \tag{B.2}$$

Changing $t = 1 - \frac{x}{R}$ we have:

$$A = \frac{1}{4} R \int_{1-\frac{x_2}{R}}^{1-\frac{x_1}{R}} [1 - \cos(\frac{\kappa^2 R(1-t)(1+t)}{4k})] dt = \frac{1}{4} R \int_{1-\frac{x_2}{R}}^{1-\frac{x_1}{R}} [1 - \cos(\frac{\kappa^2 R(1-t^2)}{4k})] dt \tag{B.3}$$

$$B = \frac{1}{4} R \int_{1-\frac{x_2}{R}}^{1-\frac{x_1}{R}} [1 + \cos(\frac{\kappa^2 R(1-t)(1+t)}{4k})] dt = \frac{1}{4} R \int_{1-\frac{x_2}{R}}^{1-\frac{x_1}{R}} [1 + \cos(\frac{\kappa^2 R(1-t^2)}{4k})] dt \tag{B.4}$$

Using a well-known trigonometric expression:

$$A = \frac{1}{4} R[2 - \cos(\frac{\kappa^2 R}{4k_0}) \int_{t_{1-}-\frac{2\Delta x}{R}}^{t_1} \cos(\frac{\kappa^2 R t^2}{4k_0}) dt - \sin(\frac{\kappa^2 R}{4k_0}) \int_{t_{1-}-\frac{2\Delta x}{R}}^{t_1} \sin(\frac{\kappa^2 R t^2}{4k}) dt] \tag{B.5}$$

$$B = \frac{1}{4} R[2 + \cos(\frac{\kappa^2 R}{4k_0}) \int_{t_{1-}-\frac{2\Delta x}{R}}^{t_1} \cos(\frac{\kappa^2 R t^2}{4k_0}) dt - \sin(\frac{\kappa^2 R}{4k_0}) \int_{t_{1-}-\frac{2\Delta x}{R}}^{t_1} \sin(\frac{\kappa^2 R t^2}{4k}) dt] \tag{B.6}$$

Changing variable again, in order to obtain the Fresnel integrals:

$$\frac{\kappa^2 R t^2}{4k} = \frac{\pi}{2} c^2 \qquad c = t\sqrt{\frac{\kappa^2 R}{2k\pi}} \qquad dt = \sqrt{\frac{2k\pi}{\kappa^2 R}} dc$$

$$\sqrt{\frac{2k\pi}{\kappa^2 R}}\int_{c_2}^{c_1}\cos(\frac{\pi}{2}c^2)dc=\sqrt{\frac{2k\pi}{\kappa^2 R}}[\int_{0}^{c_1}\cos(\frac{\pi}{2}c^2)dc-\int_{0}^{c_2}\cos(\frac{\pi}{2}c^2)dc] \quad \text{(B.7)}$$

Same for sine function.

where $C(x)=\int_0^x \cos(\frac{\pi}{2}\xi^2)d\xi$ and $S(x)=\int_0^x \sin(\frac{\pi}{2}\xi^2)d\xi$ are the *Fresnel Integral*s.

We finally reach the solution for a and B as:

$$A=\frac{1}{2}R\left\{1-\sqrt{\frac{2k_0\pi}{\kappa^2 R}}\left[C\left(\sqrt{\frac{\kappa^2 R}{2k_0\pi}}\right)\cos\left(\frac{\kappa^2 R}{4k_0}\right)+S\left(\sqrt{\frac{\kappa^2 R}{2k_0\pi}}\right)\sin\left(\frac{\kappa^2 R}{4k_0}\right)\right]\right\} \quad \text{(B.8)}$$

$$B=\frac{1}{2}R\left\{1+\sqrt{\frac{2k_0\pi}{\kappa^2 R}}\left[C\left(\sqrt{\frac{\kappa^2 R}{2k_0\pi}}\right)\cos\left(\frac{\kappa^2 R}{4k_0}\right)+S\left(\sqrt{\frac{\kappa^2 R}{2k_0\pi}}\right)\sin\left(\frac{\kappa^2 R}{4k_0}\right)\right]\right\} \quad \text{(B.9)}$$

Appendix C

NORMALIZATION FACTORS IN DFT AND IDFT

In the following appendix we explained where the coefficients used for DFT and IDFT come from.

We show mono-dimensional Fourier transforms which can be extended to 2D:

$$S(k\Delta f) = a\sum_{n=1}^{N} s(n\Delta r)e^{-j\frac{2\pi(n-1)(k-1)}{N}}\Delta r \tag{C.1}$$

$$s(n\Delta r) = b\sum_{k=1}^{N} S(k\Delta f)e^{j\frac{2\pi(n-1)(k-1)}{N}}\Delta f \tag{C.2}$$

Assuming (4.42) and substituting (C.1) in (C.2):

$$\Delta f = \frac{2\pi}{N\Delta r} \tag{C.3}$$

$$s(n\Delta r) = ab\sum_{k=1}^{N}\sum_{n=1}^{N} s(n\Delta r)e^{-j\frac{2\pi(n-1)(k-1)}{N}}\Delta r e^{j\frac{2\pi(n-1)(k-1)}{N}}\Delta f = ab\sum_{n=1}^{N} s(n\Delta r)N\frac{2\pi}{N} = abNs(n\Delta r)2\pi \tag{C.4}$$

So, to make the equality be true, the product $ab = \frac{1}{2\pi N}$. It means one could use this factor in the DFT without using any normalization in IDFT; for example.

Bibliographic References

[1] V.I Tatarskii, “The effects of the turbulent atmosphere on wave propagation”, TT-68-50464, U.S. Dept. of commerce, Springfield, VA 1971

[2] L. C. Andrews, R. L. Phillips, C. Y. Hopen, M. A. AlHabash, “Theory of optical scintillation,” J. Opt. Soc. Am. A 16,pp.1417–1429,1999

[3] J. H. Churnside, “Aperture averaging of optical scintillations in the turbulent atmosphere,” Appl. Opt. 30, pp 1982–1994, 1991.

[4] S.M. Flatté, C. Brasher, G.Wang “Probability density-functions of irradiance for waves in atmospheric turbulence calculated by numerical simulation”, J. Opt. Soc. Am. A 11, pp.2080-2092, 1994

[5] E. Vilar and J. Haddon, “Measurement and Modeling of Scintillation Intensity to Estimate Turbulence Parameters in an Earth-Space Path,” *IEEE Transactions on Antennas and Propagation*, AP-32, no. 4, 1984.

[6] D. C. Cox, H. W. Arnold, and H. H. Hoffman, “Observations of Cloud-Produced Amplitude Scintillation on 19- and 28-GHz Earth-Space Paths,” *Radio Science*, vol. 16, no. 5, 1981.

[7] E. Otung ,M. S. Mahmoud, “Rain-Induced Scintillation on Satellite Downlinks,” *Electronic Letters*, vol. 32, no. 1, 1996.

[8] D. C. Livingston, *The Physics of Microwave Propagation*, Englewood Cliffs, NJ: Prentice-Hall, 1970.

[9] Y. Karasawa and T. Matsudo, “Characteristics of Fading on Low-Elevation Angle Earth-Space Paths with Concurrent Rain Attenuation and Scintillation,” IEEE Transactions on Antennas and Propagation, vol. 39, no. 5, 1991.

[10] Feral L. “Propagation in complex media, Lecture Notes”, Université Paul Sabatier 2012

[11] Wheelon, A.D., "Electromagnetic scintillation. Part II. Weak scattering", Cambridge University Press, 2003.

[12] A.Ishimaru, “Wave propagation and scattering in random media”, Vol.2 Academic Press, New York, 1978.

[13] Th. von Karman, “Progress in the statistical theory of turbulence” Proc. Nat. Academy of Science, U.S, 34, pp. 530–539. , 1948

[14] S.M Rytov, “Diffraction of light by ultrasonic waves”, Izvestiya Akademii Nauk SSSR, Seriya Fizicheskava (Bulletin of the Academy of Science of the USSR, Phisycal Series) pp.223-259, 1937. (No english translation available)

[15] A. M. Obukhov, “On the Influence of Weak Atmospheric Inhomogeneities on the Propagation of Sound and Light,” Izvestiya Akademii Nauk SSSR, Seriya Geofizicheskaya (Bulletin of the Academy of Sciences of the USSR, Geophysical Series), 2, pp.155–165, 1953. (English translation by W. C. Hoffman, published by U. S. Air Force Project RAND as Report T-47, Santa Monica, CA, 28 July 1955.)

[16] Yu. N. Barabanenkov, Yu. A. Kravtsov, S. M. Rytov, V. I. Tatarskii, “Status of the Theory of Propagation of Waves in a Randomly Inhomogeneous Medium,” Uspekhi FizicheskikhNauk (SovietPhysics–Uspekhi), 5, pp. 551–580, 1971

[17] V. V. Pisareva. “Limits of Applicability of the Method of ‘Smooth’ Perturbations in the Problem of Radiation Propagation through a Medium Containing Inhomogeneities,” Akusticheskii Zhurnal (Soviet Physics – Acoustics), 6(1), pp. 81–86 ,1960

[18] R.L.Fante,“Electromagnetic beam propagation in turbulent media”, IEEE proc., 63, p1669, 1975

[19] Fabbro V., Feral L., “Comparison of 2D and 3D Electromagnetic approaches to Predict Tropospheric Turbulence Effects in Clear Sky Condition”, IEEE Transactions on Antennas and Propagation, in press, pp 4398-4407, 2012.

[20] R.J. Hill “Wider-angle parabolic wave equation”, J. Acoust. Soc. Am. 79(5), pp.1406-1409,1986

[21] W.A. Coles, J.P. Filice, R.G. Frehlich, M. Yadlowsky, “Simulation of wave propagation in three- dimensional random media”, App. Opt. (34)12 pp 2098-2099, 1995

[22] J.A. Rubio, A.Belmonte, A.Comeron, “Numerical simulation of long-path spherical wave propagation in three- dimensional random media” , J.Opt.Eng. 38(9) pp. 1462-1469, 1999

[23] J.M. Martin, S.M. Flatté, “Simulation of point-source scintillation through three-dimensional random media”, J. Opt. Soc. Am. A 7(5), pp.838-847, 1990

[24] L.C.Lee “Theory of thin screen scintillations for a spherical wave”, J. Astrophis 218(1), pp.468-476,1977

[25] J.M. Martin, S.M. Flatté, G.Wang “Irradiance variance of optical waves through atmospheric turbulence by numerical simulation and comparison with experiment”, J. Opt. Soc. Am. A 11, pp. 2363-2370, 1993

[26] D.L. Knepp, “Multiple phase screen calculation of the temporal behaviour of stochastic waves”, IEEE 71(6), pp.722-737, 1983

[27] A. Papoulis, “Probability, Random Variables, and Stochastic Processes” McGraw-Hill, 1965.

[28] Boulanger X., Feral L. , Castanet L. , Jeannin N. , Carrie G., Lacoste F., “A rain attenuation time-series synthesizer based on a dirac and lognormal distribution”, (section III.D), IEEE 2013

[29] Macaskill, C., T.E. Ewart, "Computer simulation of two-dimensional random wave propagation", IMA J.Appl. Math, 1984.

[30] M. Shinozuka, C.-M. Jan, “Digital simulation of random processes and its applications,” J. Sound and Vibration, 25, pp. 111-128, 1972

[31] L.E. Borgman, “Ocean wave simulation for engineering design,” ASCE, J. Waterways and Harbors Div., WW4, pp. 556-583, 1969.

[32] C.Grimault, “A multiple phase screen technique for electromagnetic wave propagation through random ionospheric irregularities”, Radio Science 33(3), pp.595-605, 1998